Title

Coordination of cortical and thalamic activity during non-REM sleep in humans.

Journal

Nature communications, 8(1)

ISSN

2041-1723

Authors

Mak-McCully, Rachel A
Rolland, Matthieu
Sargsyan, Anna
et al.

Publication Date

2017-05-01

DOI

10.1038/ncomms15499

Peer reviewed

Coordination of cortical and thalamic activity during non-REM human sleep in humans

Rachel A. Mak-McCully[1], Matthieu Rolland[2], Anna Sargsyan[2], Chris Gonzalez[1], Michel Magnin[3], Patrick Chauvel[4,5,6], Marc Rey[4,5,6]†, Hélène Bastuji[3,7]†, Eric Halgren[1,2,8]†*

[1]Department of Neurosciences, University of California, San Diego, California, 92093, USA.
[2]Department of Radiology, University of California, San Diego, California, 92093, USA.
[3]Central Integration of Pain, Lyon Neuroscience Research Center, INSERM, U1028; CNRS, UMR5292; Université Claude Bernard, Lyon, Bron, France.
[4]Aix-Marseille Université, 13385, Marseille, France.
[5]INSERM, Institut de Neurosciences des Systèmes UMR 1106, 13005, Marseille, France.
[6]APHM (Assistance Publique–Hôpitaux de Marseille), Timone Hospital, 13005, Marseille, France.
[7]Unité d'Hypnologie, Service de Neurologie Fonctionnelle et d'Épileptologie, Hôpital Neurologique, Hospices Civils de Lyon, Bron, France.
[8]Department of Psychiatry, University of California, San Diego, California, 92093, USA.

† Co-senior authors

* Correspondence to: ehalgren@ucsd.edu

Abstract

Every night, the human brain produces thousands of downstates and spindles during non-REM sleep. Previous studies indicate that spindles originate thalamically, and downstates cortically, loosely grouping spindle occurrence. However, the mechanisms whereby the thalamus and cortex interact in generating these sleep phenomena remain poorly understood. Using bipolar depth recordings, we report here a sequence wherein: 1) convergent cortical downstates lead thalamic downstates; 2) thalamic downstates hyperpolarize thalamic cells, thus triggering spindles; and 3) thalamic spindles are focally projected back to cortex, arriving during the down-to-upstate transition when the cortex replays memories. Thalamic intrinsic currents, therefore, may not be continuously available during non-REM sleep, permitting the cortex to control thalamic spindling by inducing downstates. This archetypical cortico-thalamo-cortical sequence could provide the global physiological context for memory consolidation during non-REM sleep.

Introduction

A fundamental characteristic of mammalian brains is the predominance of ~0.5-4Hz slow waves and 0.5-2s bursts of 10-16Hz spindles during non-REM (NREM) sleep. These rhythms control corticothalamic activity, including cell-firing and plasticity, during ~25% of our lives. Slow waves are composed of a downstate, characterized by a period of hyperpolarization, followed by an upstate, characterized by a period of firing near waking levels (*1*). Physiologically, slow wave downstates are stereotyped, while the upstate exhibits more variability (*2*). Spindles are generated in the thalamus by powerful intrinsic H (called the pacemaker current, I_h) and T (low voltage calcium, I_T) currents, and the local circuit between thalamocortical and thalamic reticular nucleus cells (*3*). During NREM sleep, the thalamus is commonly thought to be in a hyperpolarized state that permits activation of I_h, I_T, and rhythmic burst firing, allowing spindles to spontaneously emerge (*4*).

Although spindles arise primarily thalamically (*5*), and slow waves cortically (*6*), they each clearly involve both structures (*7-9*). Earlier studies described the grouping of spindles by slow waves in the anesthetized cat cortex and thalamus (*10*), in EEG recordings (*11*), and in medial depth recordings in humans (*12*). This grouping of spindles by slow waves may hierarchically organize memory replay originating in the hippocampus: firing patterns encoding memories are replayed during hippocampal sharp waves and ripples, which are associated with cortical spindles and down-to-upstate transitions in rats (*13-16*). Recently, this hippocampal-cortical coordination was confirmed to underlie memory consolidation (*17*). In humans, hippocampal ripples may be grouped by local spindles and slow waves (*18*). Behaviorally, memory consolidation is correlated with the coordination of spindles with slow waves in human EEG (*19*). Here, we demonstrate and quantify the ordered co-occurrence of spindles and downstates in the human cortex and thalamus. Our findings suggest strong functional interactions enabling a structured neurophysiological environment to emerge during memory replay in humans.

Results

Downstates and spindles were detected on 22 cortical and eight thalamic, mainly pulvinar, bipolar channels during NREM stages 2 & 3 (N2 & N3) in three patients undergoing evaluation for epilepsy. Using bipolar derivations ensured that the recorded activity was generated in the local thalamic or cortical gray matter immediately surrounding the contacts. The detected downstates and spindles, therefore, arose in the indicated locations and were not the result of volume conduction (*20*). Downstates occurred on average more frequently in the cortex (16.3±1.1/minute/channel) versus thalamus (11.5±2.2, two-way ANOVA comparing downstate densities and spindle densities of the 22 cortical and 8 thalamic channels, main effect of sleep event type, $p<0.0001$), while spindles occurred more frequently in the thalamus (7.1±1.8) versus cortex (5±1.3, two-way ANOVA, $p<0.0001$; Supplementary Table 2). Although the area sampled is limited, these results, together with the earlier latency of downstates in the cortex and of spindles in the thalamus (see "Cortical downstates lead thalamic downstates" and "Thalamic spindles lead cortical spindles" below) support previous suggestions that the cortex generally initiates downstates and the thalamus initiates spindles.

Cortical downstates lead thalamic downstates

Cortical downstate peaks significantly led thalamic downstate peaks in simultaneously recorded corticothalamic pairs (Figs. 1A-C&F & Supplementary Figure 2a). Fifty percent of the 64 pairs exhibited a significant temporal order; of these, ~90% showed a significant temporal order from the cortex to the thalamus (binomial tests significant at $p<.05$ after Bonferroni correction; see Supplementary Table 3A for all significant pairs and p-values). Critically, a thalamic downstate was more likely to occur if the number of cortical channels participating in the downstate was two (Fig. 1G & Supplementary Note 1) or more (Supplementary Note 1 & Supplementary Figure 3), compared to when a single channel participated. Due to the cortex's depolarizing influence on thalamic neurons, cortical downstates, particularly those involving multiple locations, would disfacilitate (i.e. lack the depolarizing drive from the cortex onto thalamic neurons) thalamic neurons, and may thereby induce thalamic downstates. Cortical downstates in humans are highly variable in their location, extent, and synchronization (*20*). In significant cortical-to-thalamic pairs, the average delay from cortical downstate peak to thalamic

downstate peak was 218±66ms, presumably reflecting the integration time needed for the disfacilitating influences of the temporally-dispersed cortical downstates to summate on their thalamic targets.

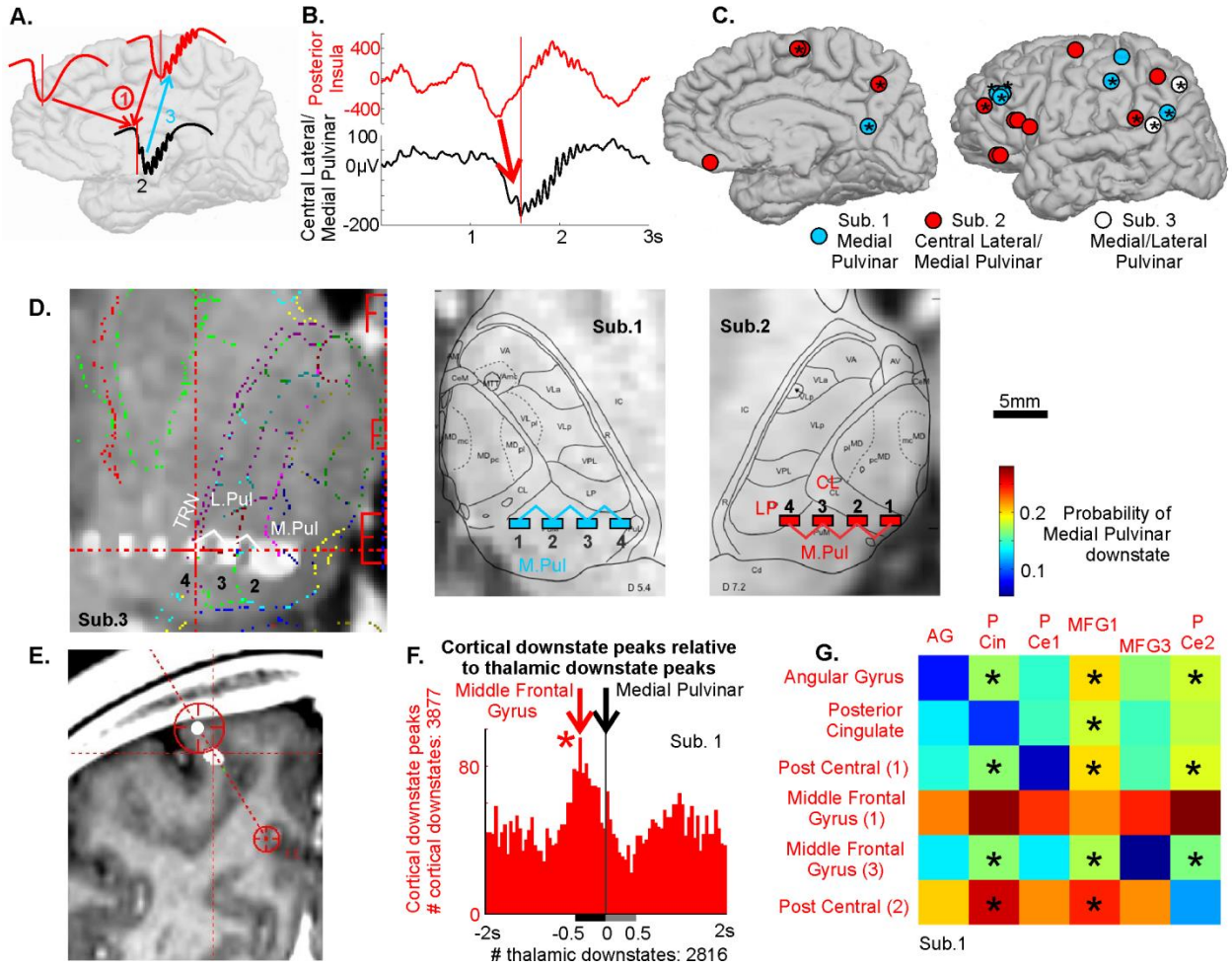

Figure 1. Cortical downstates lead thalamic downstates. A. Overall schema: 1) Cortical downstate convergence leads to thalamic downstates; 2) thalamic downstates produce thalamic spindles; and 3) thalamic spindles drive cortical spindles. B. Single trial example of a cortical downstate leading a thalamic downstate. C. Cortical recording sites. Asterisks indicate cortical locations whose downstates significantly lead downstates in one particular thalamic site, indicated by label, paired to each subject's cortical channels (color-coded). D. Thalamic recording sites. E. Example transcortical bipolar pair. F. Thalamic downstate peaks are locked at 0ms (vertical black line) and the number of cortical downstate peaks occurring within ±2s are plotted in red 50ms bins. Cortical downstates occur significantly (*) more often before thalamic downstates than after (Supplementary Table 3a). Representative corticothalamic pair; additional examples in Supplementary Figure 2a. Similar results were obtained in N2 and N3 (Supplementary Tables 4a & 5a). G. Thalamic downstate probability significantly increases when two cortical locations, compared to one, produce a downstate. Boxes along the diagonal show the probability of a medial pulvinar downstate peak occurring within 500ms after a cortical downstate peak in the cortical channel listed to the left. The remaining boxes indicate the

probability of a medial pulvinar downstate peak occurring within 500ms after a cortical downstate peak in the cortical channel listed to the left, given a downstate in the cortical channel listed on top also occurs within 500ms after the cortical channel listed to the left (*=p<0.05, Chi-square, Bonferroni corrected).

Thalamic downstates control thalamic spindle onset

Given current models of thalamic spindle generation, we were surprised to observe that thalamic downstates tightly controlled thalamic spindling (Fig. 2 & Supplementary Figure 4). During NREM sleep, the thalamus operates in a burst firing mode governed by the interaction of thalamic I_h and I_T (*3*). Adequate hyperpolarization is required to de-inactivate I_T and activate I_h. Subsequent I_T activation leads to a low-threshold calcium spike crowned by action potentials. As a population, this burst firing in thalamocortical and thalamic reticular neurons generates the 10-16Hz oscillations underlying spindles. Consequently, the hyperpolarized state of the thalamus during NREM sleep should spontaneously generate spindles, regardless of the presence or absence of downstates. In contrast, we find that the thalamic downstate tightly controls spindle onset in all eight thalamic channels (Fig. 2b & Supplementary Figure 4, left columns). The normalized proportion of spindles occurring with downstates in the thalamus (0.63±0.21) is nearly double that in the cortex (0.38±0.07, p=0.005, one-tailed two sample t-test, unequal variance, 8 thalamic channels and 22 cortical channels), as is the enrichment factor of spindle density around downstates (5.62±2.13 in the thalamus versus 3.15±0.9 in the cortex, p=0.007, one-tailed two sample t-test, unequal variance, 8 thalamic channels and 22 cortical channels) (Supplementary Table 6).

We interpret these results as indicating that thalamocortical cells are not sufficiently hyperpolarized during NREM sleep to de-inactivate I_T and activate I_h. Rather, they require the additional hyperpolarization produced by the downstate. A corollary of this view is that spindles terminate when the thalamus returns to its baseline NREM membrane potential at the end of the downstate. Indeed, plots of thalamic spindle termination versus downstates support this effect (Fig. 2b & Supplementary Figure 4, second columns). Conversely, the start of the spindle appears to begin the transition from the down-to-upstate, as would be expected from the strong depolarizing currents which spindles engage. As thalamic downstates appear to be induced by cortical downstates, and thalamic downstates are tightly coupled to the production of thalamic spindles, this allows the cortex a degree of control over thalamic spindle occurrence.

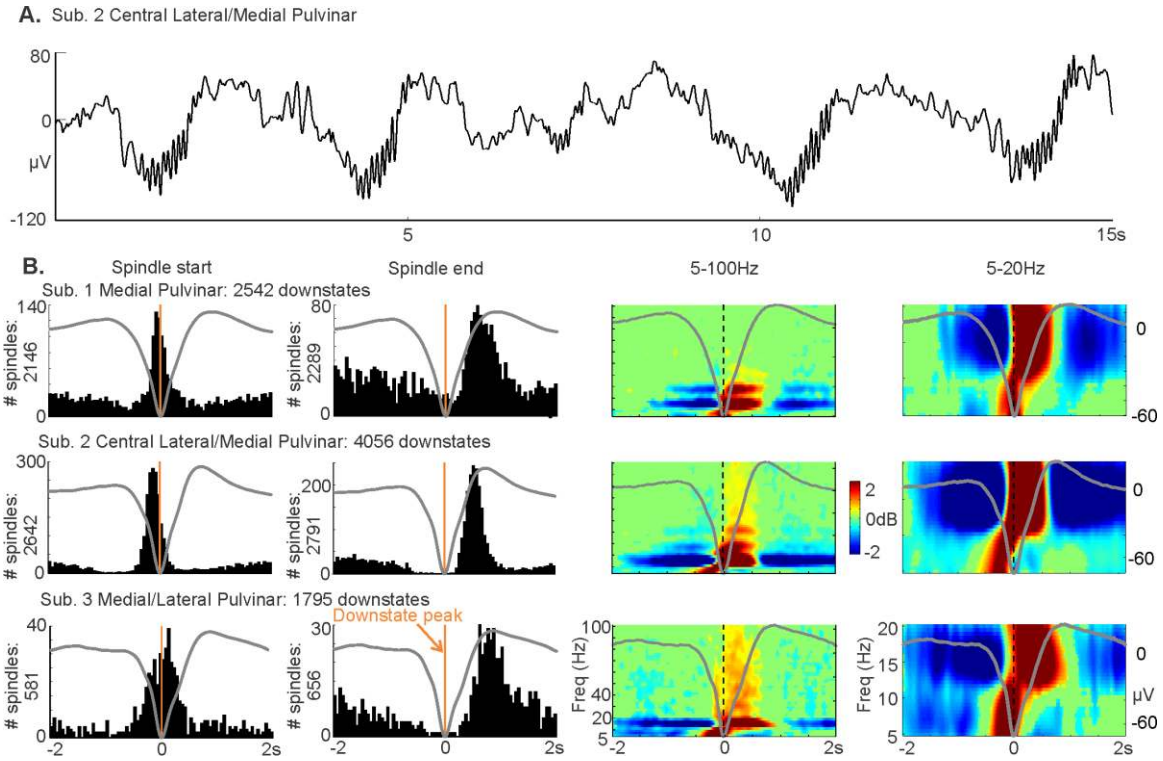

Figure 2. Thalamic downstates trigger thalamic spindles. Spindles start, on average, at the thalamic downstate peak, and end near the following upstate peak. A. Representative single trace. B. Histograms of thalamic spindle onsets (first column) or spindle terminations (second column) in relation to the thalamic downstate peak at 0ms (vertical orange line) for each thalamic channel; counts in 50ms bins. Waveforms show the averaged local field potential in each channel. Spectral power from 5-100Hz (third column), or from 5-20Hz (fourth column), averaged on the downstate peaks at 0ms, baseline corrected over entire epoch, thresholded at $p<0.01$, uncorrected. Representative channels; additional channels in Supplementary Figure 4. Similar results were obtained in N2 and N3 (Supplementary Figures 5-7) and with stricter downstate detection parameters (Supplementary Figure 11).

Thalamic spindles lead cortical spindles

In contrast to the consistent lead of cortical downstates over thalamic downstates, thalamic spindle onsets lead those of cortical spindles: 42% of thalamocortical pairs showed a significant temporal order, with the thalamus leading in all (Fig. 3a&b, Supplementary Figure 2b, & Supplementary Table 3b). Figure 3c-e demonstrates the focal driving of annectant gyrus spindles by the medial/lateral pulvinar: 98% of detected pulvinar spindles overlapped with detected (81%) or candidate (17%) annectant spindles (Fig. 3c&d; candidate epochs met minimum amplitude-duration criteria, see Methods, "Current spindle detection method"). Spindles were considered overlapping between the two channels if any part of a spindle in one channel overlapped at any point in time with a spindle in the second channel. In this pair, high gamma associated with 15,205 spindle troughs in the pulvinar preceded that in the annectant gyrus after ~15ms (Fig. 3e, 14.7ms significantly different than zero; two-tailed paired t-test between the time of cortical high gamma amplitude peaks compared to zero and the time of the thalamic high gamma amplitude peaks compared to zero over all subsets of 500 spindle peaks,

p=0.00035). Overall, these results indicate that thalamic spindles consistently lead cortex spindles, and are consistent with the thalamus focally driving spindle production in certain connected cortical areas (see Supplementary Note 2 and Supplementary Figure 8 for additional examples of corticothalamic functional connectivity).

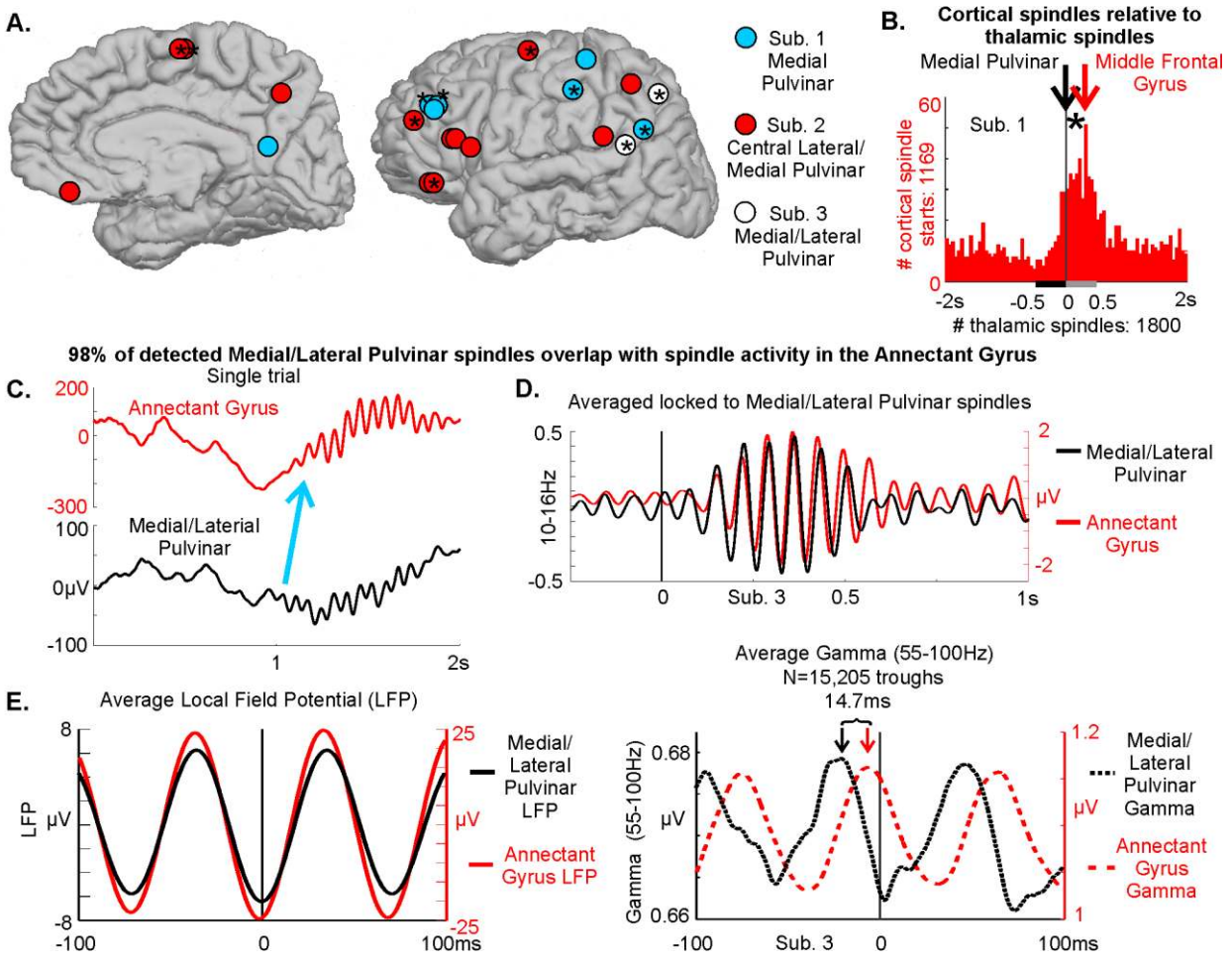

Figure 3. Thalamic spindles lead cortical spindles. A. Cortical sites. Asterisks indicate cortical locations where thalamic spindles significantly lead cortical spindles, in a particular thalamic site/subject. B. Thalamic spindle onsets are locked at 0ms (vertical black line) and the number of corresponding cortical spindle onsets occurring within ±2s are plotted in red 50ms bins. Cortical spindles occur significantly (*) more often after thalamic spindles than before (Supplementary Table 3b). Representative corticothalamic pair; additional examples in Supplementary Figure 2b. Similar results were obtained in N2 and N3 (Supplementary Tables 4b & 5b). C. Single trial of overlapping medial/lateral pulvinar and annectant gyrus spindles. D. Bandpassed (10-16Hz) average of the 81% overlapping detected spindles, locked to the pulvinar spindle onsets (vertical black line), indicating synchronous spindle occurrence. E. In the same pair, locked to individual pulvinar spindle troughs (black trace) in the local field potential (LFP), the averaged cortical LFP spindle troughs are synchronous to the pulvinar (left); however, the corresponding high gamma amplitude in the pulvinar leads the cortex by 14.7ms (right).

Cortical spindles arrive during down-to-upstate transition

When spindles arrive in the cortex from the thalamus, they arrive during the cortical down-to-upstate transistion (Fig. 4a & Supplementary Figure 9), with a sharp peak in spindle onset occurring ~250ms after the downstate peak (Fig. 4b). These findings are consistent across cortical locations (Fig. 4a & Supplementary Figure 9) as well as for both slow (>10 and ≤12Hz) and fast (>12 and <16Hz) spindles (Fig. 4b).

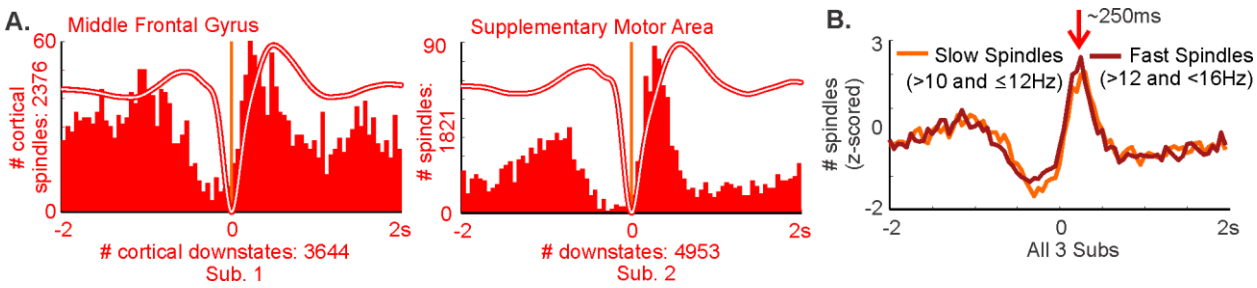

Figure 4. Cortical spindles start during the cortical down-to-upstate transition. A. Histograms of cortical spindle onsets in relation to the cortical downstate peak at 0ms (vertical orange line) for each cortical channel in 50ms bins. Waveforms show the averaged local field potential in each channel. Representative channels; additional channels in Supplementary Figure 9. Cortical spindle onset occurs during the down-to-upstate transition in the cortex. Similar results were obtained in N2 and N3 (Supplementary Figures 5-7) and with stricter downstate detection parameters (Supplementary Figure 10). B. Both slow and fast spindles occur on the down-to-upstate transition in the cortex. Results are z-scored on 17 channels in which at least 100 slow (>10 and ≤12Hz) spindles occurred within ± 500ms of a downstate and on 12 channels in which at least 100 fast (>12 and <16Hz) spindles occurred within ± 500ms of a downstate. The red arrow indicates the point, around 250ms after the cortical downstate, when both slow and fast cortical spindles show a peak in start times.

Proposed model

Taken together, our results suggest a sequential cortico-thalamo-cortical sequence of downstates and spindles (Fig. 5): cortical downstates lead thalamic downstates; the hyperpolarization caused by thalamic downstates triggers thalamic spindle onsets; thalamic spindles lead cortical spindles, driving individual spindle troughs in connected thalamocortical pairs; and cortical spindles arrive in the cortex during the cortical down-to-upstate transition.

Discussion

During the course of a night's sleep, the human brain produces thousands of downstates and spindles. Yet, we still lack a basic understanding of what triggers these events, and how they are coordinated across different brain regions. Here, using rare simultaneous bipolar SEEG recordings in the human thalamus and cortex, we quantify the local generation and interaction of these events between the thalamus and cortex. While previous studies have observed the grouping of spindles by slow waves, this is the first demonstration and quantification of the temporal order of these sleep events as they occur within and between the human thalamus and

cortex. Rather than independent origin of downstates and spindles in the cortex and thalamus, respectively, we find that downstates and spindles occur in a highly regular temporal sequence, both within and between structures. We interpret the implied interactions as arising from the known connections between and within these structures, as well as the powerful voltage-gated channels previously shown in animals to be key for the generation of thalamic spindles.

Our findings appear to be inconsistent with the widespread assumption that the thalamic currents are continuously available during NREM; rather, we propose that these currents become available when downstates hyperpolarize the thalamus, thus allowing spindles to emerge. We show that thalamic downstates systematically follow cortical downstates, and are especially likely when downstates occur in multiple cortical locations, suggesting that the abrupt silencing of depolarizing projections from the cortex ('disfacilitation') may induce thalamic downstates. Since thalamic downstates themselves trigger thalamic spindles, this provides a mechanism whereby the cortex may indirectly trigger thalamic spindles. We also show that thalamic spindles begin before cortical spindles, both as the overall spindle envelope, and as individual oscillations, consistent with current models wherein thalamic spindles drive cortical spindles. In sum, we interpret our data as indicating that converging cortical downstates induce thalamic downstates, thalamic downstates release thalamic spindles, and thalamic spindles drive cortical spindles. Thalamic spindles begin at the peak of the thalamic downstate, but since this is delayed from the cortical downstate, cortical spindles begin about midway between the down and upstate peaks, when cortical activity networks are re-forming. We propose that this heretofore undescribed interaction between cortex and thalamus can control the initiation and timing of downstates and spindles in order, we hypothesize, to support memory consolidation. There are other interpretations of our data, which we discuss below.

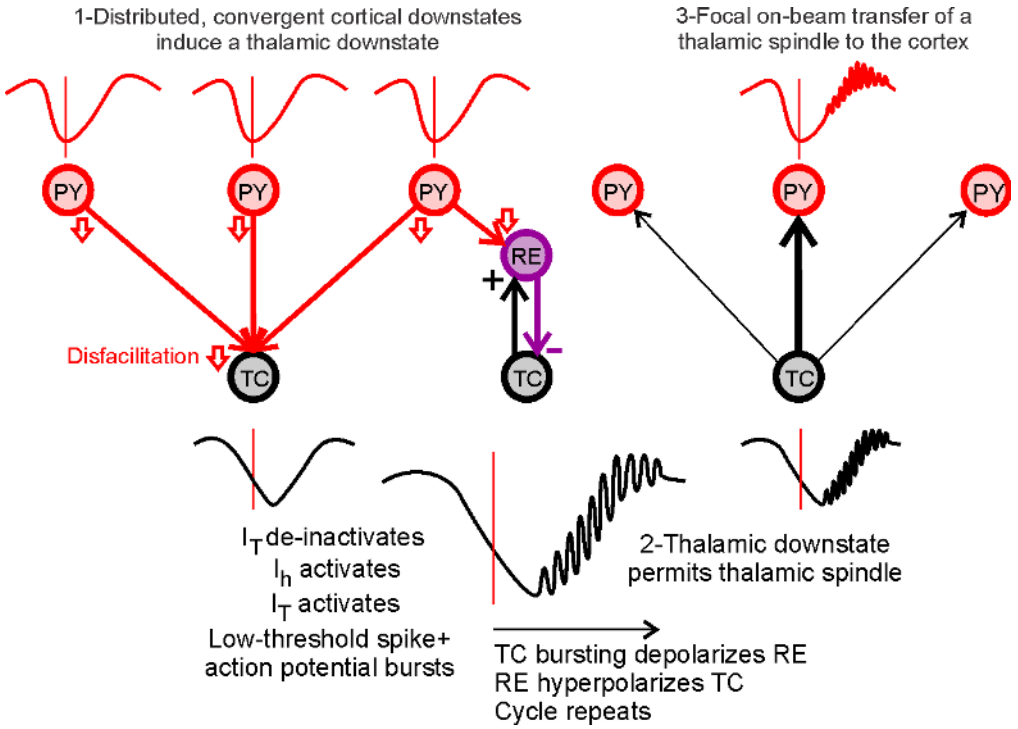

Figure 5. Proposed model for how corticothalamic coordination produces downstates and spindles during NREM sleep. Convergence of cortical downstates produces thalamic

hyperpolarization (i.e. a downstate) by removing depolarizing input from the cortex (i.e., disfacilitation, open red arrows; see Fig. 1). This thalamic hyperpolarization de-inactivates I_T and activates I_h, evoking a thalamic spindle that is reinforced by rhythmic feedback inhibition from thalamic reticular neurons (see Fig. 2). The thalamic spindle, in turn, is focally projected to the cortex (see Fig. 3), arriving during the cortical down-to-upstate transition (see Fig. 4). PY=pyramidal; TC=thalamocortical; RE=thalamic reticular.

We found that cortical downstates may induce thalamic downstates: in ~90% of corticothalamic channel pairs with a significant order, the cortical downstate led the thalamic downstate. Furthermore, downstates occurred ~50% more often (on a per channel basis) in the cortex than thalamus. Finally, a thalamic downstate was more likely to occur if two or more cortical channels generated a downstate, than if only one did. We interpret these observations as being consistent with cortical downstates inducing thalamic downstates via disfacilitation. Cortical pyramidal cells have a relatively high spontaneous firing rate in NREM sleep between downstates, but stop firing (completely or nearly so) during downstates (*21*). Thalamocortical projection (TC) cells receive their main excitatory input from the cortex. Removal of this excitatory drive during a cortical downstate (i.e., disfacilitation) would be expected to hyperpolarize TC cells, and thus could induce a downstate. Note that this disfacilitation would also occur in the nucleus reticularis (RE), whose cells inhibit TC cells. The consequent potential disynaptic disinhibition could be relatively powerful (*22*) and perhaps overcome the monosynaptic disfacilitation. In this case, it would be difficult to explain the association of thalamic downstates with cortical downstates, the strong tendency of thalamic downstates to follow cortical downstates, and the accentuation of that tendency when more cortical downstates are present. One possibility that might produce this paradoxical combination if the disynaptic pathway were dominant would be if the cortical projection to RE disrupted ongoing spindle oscillations, which would then decrease TC activity, as we showed in a modeling study (*23*). However, this mechanism requires that thalamic spindles precede thalamic downstates, but we found that they follow.

In contrast to this interpretation, we propose that the disynaptic pathway from cortex to TC cells via RE is not immediately engaged by cortical downstates. Note that disfacilitation of RE would only have indirect effects on TC if RE were spontaneously active during NREM sleep, and limited observations in rats suggest that this is not the case (*24*). This interpretation is supported by the lack of high gamma activity in the thalamus before the downstate in our data, as evidenced by the lack of a decrease of high gamma during the downstate relative to baseline. We conclude that hyperpolarizing downstates in both TC and RE neurons due to converging disfacilitation from cortical downstates is the interpretation most consistent with our findings and the current literature, but this possibility needs to be directly tested.

. We also found that thalamic downstates may release thalamic spindles. When thalamic cells are sufficiently hyperpolarized, the I_h and I_T currents become available (*3*). I_h slowly depolarizes the cell, until I_T is opened, causing a burst of action potentials, followed by rebound hyperpolarization due to intrinsic currents and inhibitory feedback from RE. Recovery of I_T, as well as from the after-hyperpolarization due to I_h and cortical feedback, leads to the next spindle wave. In current theories of thalamic spindle generation (*25*), it is assumed that the I_h and I_T

currents are available quasi-continuously during NREM sleep, and so spindles are triggered by small random excitatory fluctuations, resulting in nearly continuous spindling separated by refractory periods. In contrast, based on the very strong association of thalamic spindles with local downstates, their onset times being tightly clustered on the downstate peak, we propose that the I_h and I_T currents do not become available until the thalamus enters a downstate.

One objection to our proposal is that not all thalamic spindles are tightly coupled to thalamic downstates. It is possible that downstate-like hyperpolarizing fluctuations, which are not captured by our selection criteria, occur with these non-coupled spindles. This possibility is supported by the similar results we obtained across a two-fold range of thalamic downstate detection thresholds (bottom 40% and bottom 20% of peaks). Extending this view, it is consistent with our data to suppose that the membrane potential of thalamic cells during NREM sleep are close enough to the level where I_h and I_T become available that very small fluctuations can release spindles in the absence of a detectable downstate. One might expect in this case that the delay from downstate onset to spindle onset would be shorter than the ~500ms which we observed. However, this delay may be due to the long time required to de-inactivate I_T and activate I_h channels which had been inactivated by depolarization (*26*).[add T ref like lambert]

Alternatively, it is possible the non-coupled spindles are generated in another part of the thalamus, where they were coupled to a downstate, and then propagated to where we were recording. The limited anatomical sampling is a general constraint on our interpretations. Finally, it is conceivable that I_h and I_T are continuously available during NREM sleep, and other mechanisms operate to trigger thalamic spindles at the downstate peak, and to suppress spindles in the periods between downstates. For example, a third structure may project to both the thalamus and cortex, causing downstates and then spindles. In order to account for our data, the downstate-triggering input would need to be projected to the cortex before the thalamus, and the spindle-triggering input would need to be projected to the thalamus before the cortex. Alternatively, some aspect of the down-to-upstate transition may trigger spindles independently in both structures, but at different latencies (immediately in the thalamus and after a 250ms delay in the cortex). We are not aware of inputs or mechanisms which satisfy these requirements.

We additionally observed that thalamic spindles may drive cortical spindles. Thalamic and cortical spindles tended to overlap, and in all cases where there was a significant order in their onset, the thalamic spindles led the cortical. Furthermore, when examining those thalamocortical pairs that appear to be directly connected, there is a nearly one-to-one overlap between the thalamic and cortical spindles. In such a case, the oscillations in high gamma accompanying the spindles in the thalamus significantly led those in the cortex. Since broadband high gamma amplitude is highly correlated with population firing (*27*), and since the ~15ms delay during spindles from thalamus to cortex is comparable to the thalamocortical conduction delay estimated from auditory evoked potentials (*28*), these observations are consistent with spindles arising in the thalamus and being projected to the cortex. Furthermore, association of spindles with downstates is much stronger in the thalamus than in the cortex, which is what would be expected if spindles are generated in the thalamus in response to downstates, and then are projected to the cortex.

Our interpretation that human sleep spindles are initiated in the thalamus and then projected to the cortex is consistent with the effects of lesions in mammals (*5, 29*). However, an alternative interpretation has been proposed, wherein cortical spindles are gated by the depolarization occurring during the cortical upstate (*30*), which is assimilated into a more general

tendency of higher frequency oscillations to be gated by lower. Support for this interpretation is the previous observation that the midpoint of human sleep spindles at the scalp tends to peak at the midpoint of upstates (*11, 12*). Since we are concerned with spindle initiation, we related spindle onset to slow waves in the cortex, and found that their peak is about midway between down- and upstate peaks. This is in contrast to the thalamus, where spindle onsets are centered on the downstate peaks. Note that thalamic downstates peak ~200ms after cortical, so cortical spindles occur only shortly after thalamic. Thus, our model provides a consistent mechanistic explanation for the associations and timings of downstates and spindles in thalamus and cortex. However, again, one could posit a third structure which induces down- and upstates in the cortex and thalamus, as well as initiates spindles, with the requisite timing and correlations.

The recordings and analyses presented here have a number of limitations. Recordings in the thalamus were clearly different than those in the cortex: the thalamic recordings were much lower in amplitude, had small gamma fluctuations, and were largely dominated by clear spindles, often occurring in tandem with slow waves. Identification of thalamic downstates was also not as straightforward as in the cortex, due to the difficulty of identifying polarity in relation to high gamma changes (see Methods for details). The thresholds used in previous detection methods for cortical slow waves and spindles did not adequately recognize the discrete events seen in the raw thalamic data. In order to address this issue, we took the bottom 40% of slow waves as downstates compared to the 20% used in previous methods (*12, 31*). However, when we reanalyze our results using only the bottom 20% of downstates, our results still show the same thalamocortical relationships. Our spindle detection method, detailed in the Methods section, optimized spindle detection on a per channel basis, outperforming the previous standard method. Performance of the methods was validated by extensive visual inspection of individual channels and traces.

Additionally, the time between zero crossings used for downstate detection (0.25 to 3secs) means that the downstates analyzed here were between ~0.16 to 2Hz. Studies in anesthetized cats suggests a difference between slow oscillations (<1Hz) and delta waves (1-4Hz) (*6*); however, human laminar recordings indicate that the LFP gradient, multi-unit activity and CSD profile are similar from 0.6-2Hz (*21*).

Simultaneous recordings in the human thalamus and cortex are extremely rare and only occur in patients with a clinical necessity for such recordings. In the work presented here, all implanted subjects were patients with pharmaco-resistant epilepsy. In order to exclude as much as possible the influence of epilepsy on our analyses, our inclusion criteria were extremely conservative. Patients and channels were excluded if there was evidence of extensive epileptic activity (see Methods). Time periods in which brief epileptic activity was suspected were also excluded from analysis. Furthermore, the patients studied here presented with temporal lobe epilepsy and seizures related to this type of epilepsy tend to occur during wakefulness rather than sleep (*32*). Finally, also due to the limited nature of these recordings, our sample size is limited both in terms of number of subjects, as well as number of sites. Our cortical coverage is small and our thalamic leads largely confined to the pulvinar. However, given this small sample size, it is still remarkable to find highly consistent temporal relationships between cortical and thalamic spindles and downstates. This implies a global structure of cortico-thalamo-cortical interactions that holds across the cortical mantle.

Studies in humans strongly suggest that memory consolidation occurs during sleep because manipulating the amount of graphoelements produced during sleep can enhance performance: for example, inducing slow oscillations via transcranial stimulation (*33*) or

increasing spindle density with zolpidem (*34*) improves declarative memory; recently, memory consolidation in humans was found to be highly correlated with the occurrence of spindles at down-to-upstate transitions detected in scalp EEG (*19*). Furthermore, this effect may occur very locally (*35*).

Hippocampal-dependent declarative memories are thought to be replayed during sleep in order to move the memory to the cortex for long term storage (*36*). Hippocampal ripples produced in CA1 and sharp waves generated in CA3 are thought to underlie this memory replay process. In rats, KCs have been shown to group these replay periods (*37*) and KCs, downstates & high voltage spikes have also been correlated with replay (*15*). Ripples have also been correlated with cortical slow activity and spindles (*38*), and sharp waves are thought to be grouped by the cortical slow wave (*13*). Using stimulation, hippocampal-cortical coordination via sharp wave-ripples, delta oscillations and ripples, has been demonstrated to underlie memory consolidation (*17*). Given the strong anatomical projections from thalamus to hippocampus, it is possible that thalamic spindles also drive hippocampal spindles, in parallel to the thalamocortical driving demonstrated here, but direct evidence is lacking.

In summary, our results reveal a dynamic cortico-thalamo-cortical loop temporally coordinating downstates and spindles during human NREM sleep. The cortex is silent at the beginning of this transition and achieves waking firing levels at its end (*39*). Our results suggest a mechanism whereby the cortico-thalamo-cortical connections and intrinsic thalamic channel properties interact to ensure that spindles arrive at the cortex when this cortico-cortical associative network is being constructed. We hypothesize that this loop may help organize memory replay.

References

1. M. Steriade, A. Nunez, F. Amzica, A novel slow (< 1 Hz) oscillation of neocortical neurons in vivo: depolarizing and hyperpolarizing components. *Journal of Neuroscience.* **13**, 3252-3265 (1993).
2. J. Y. Chen, S. Chauvette, S. Skorheim, I. Timofeev, M. Bazhenov, Interneuron-mediated inhibition synchronizes neuronal activity during slow oscillation. *J Physiol.* **590**, 3987-4010 (2012).
3. D. A. McCormick, T. Bal, Sleep and arousal: thalamocortical mechanisms. *Annual Review of Neuroscience.* **20**, 185-215 (1997).
4. D. A. McCormick, M. J. McGinley, D. B. Salkoff, Brain state dependent activity in the cortex and thalamus. *Current Opinion in Neurobiology.* **31**, 133-140 (2015).
5. R. S. Morison, D. L. Bassett, *Electrical activity of the thalamus and basal ganglia in decorticate cats*. (1945), vol. 8, pp. 309-314.
6. M. Steriade, A. Nunez, F. Amzica, Intracellular analysis of relations between the slow (< 1 Hz) neocortical oscillation and other sleep rhythms of the electroencephalogram. *J Neurosci.* **13**, 3266-3283 (1993).
7. F. David, J. T. Schmiedt, H. L. Taylor, G. Orban, G. Di Giovanni, V. N. Uebele, J. J. Renger, R. C. Lambert, N. Leresche, V. Crunelli, Essential thalamic contribution to slow waves of natural sleep. *Journal of Neuroscience.* **33**, 19599-19610 (2013).

8. M. Lemieux, J. Y. Chen, P. Lonjers, M. Bazhenov, I. Timofeev, The impact of cortical deafferentation on the neocortical slow oscillation. *Journal of Neuroscience.* **34**, 5689-5703 (2014).
9. M. Bonjean, T. Baker, M. Lemieux, I. Timofeev, T. Sejnowski, M. Bazhenov, Corticothalamic feedback controls sleep spindle duration in vivo. *Journal of Neuroscience.* **31**, 9124-9134 (2011).
10. D. Contreras, M. Steriade, Cellular basis of EEG slow rhythms: a study of dynamic corticothalamic relationships. *Journal of Neuroscience.* **15**, 604-622 (1995).
11. M. Molle, L. Marshall, S. Gais, J. Born, Grouping of spindle activity during slow oscillations in human non-rapid eye movement sleep. *Journal of Neuroscience.* **22**, 10941-10947 (2002).
12. T. Andrillon, Y. Nir, R. J. Staba, F. Ferrarelli, C. Cirelli, G. Tononi, I. Fried, Sleep spindles in humans: insights from intracranial EEG and unit recordings. *Journal of Neuroscience.* **31**, 17821-17834 (2011).
13. F. P. Battaglia, G. R. Sutherland, B. L. McNaughton, Hippocampal sharp wave bursts coincide with neocortical "up-state" transitions. *Learn Mem.* **11**, 697-704 (2004).
14. A. G. Siapas, M. A. Wilson, Coordinated interactions between hippocampal ripples and cortical spindles during slow-wave sleep. *Neuron.* **21**, 1123-1128 (1998).
15. L. A. Johnson, D. R. Euston, M. Tatsuno, B. L. McNaughton, Stored-trace reactivation in rat prefrontal cortex is correlated with down-to-up state fluctuation density. *Journal of Neuroscience.* **30**, 2650-2661 (2010).
16. M. Molle, O. Yeshenko, L. Marshall, S. J. Sara, J. Born, Hippocampal sharp wave-ripples linked to slow oscillations in rat slow-wave sleep. *Journal of Neurophysiology.* **96**, 62-70 (2006).
17. N. Maingret, G. Girardeau, R. Todorova, M. Goutierre, M. Zugaro, Hippocampo-cortical coupling mediates memory consolidation during sleep. *Nature Neuroscience.* (2016).
18. B. P. Staresina, T. O. Bergmann, M. Bonnefond, R. van der Meij, O. Jensen, L. Deuker, C. E. Elger, N. Axmacher, J. Fell, Hierarchical nesting of slow oscillations, spindles and ripples in the human hippocampus during sleep. *Nat Neurosci.* (2015).
19. M. Niknazar, G. P. Krishnan, M. Bazhenov, S. C. Mednick, Coupling of Thalamocortical Sleep Oscillations Are Important for Memory Consolidation in Humans. *PLoS One.* **10**, e0144720 (2015).
20. R. A. Mak-McCully, B. Q. Rosen, M. Rolland, J. Regis, F. Bartolomei, M. Rey, P. Chauvel, S. S. Cash, E. Halgren, Distribution, Amplitude, Incidence, Co-Occurrence, and Propagation of Human K-Complexes in Focal Transcortical Recordings(1,2,3). *eNeuro.* **2**, (2015).
21. R. Csercsa, B. Dombovari, D. Fabo, L. Wittner, L. Eross, L. Entz, A. Solyom, G. Rasonyi, A. Szucs, A. Kelemen, R. Jakus, V. Juhos, L. Grand, A. Magony, P. Halasz, T. F. Freund, Z. Magloczky, S. S. Cash, L. Papp, G. Karmos, E. Halgren, I. Ulbert, Laminar analysis of slow wave activity in humans. *Brain.* **133**, 2814-2829 (2010).
22. E. G. Jones, Synchrony in the interconnected circuitry of the thalamus and cerebral cortex. *Annals of the New York Academy of Sciences.* **1157**, 10-23 (2009).
23. R. A. Mak-McCully, S. R. Deiss, B. Q. Rosen, K. Y. Jung, T. J. Sejnowski, H. Bastuji, M. Rey, S. S. Cash, M. Bazhenov, E. Halgren, Synchronization of isolated downstates (K-complexes) may be caused by cortically-induced disruption of thalamic spindling. *PLoS Comput Biol.* **10**, e1003855 (2014).

24. P. Bartho, A. Slezia, F. Matyas, L. Faradzs-Zade, I. Ulbert, K. D. Harris, L. Acsady, Ongoing network state controls the length of sleep spindles via inhibitory activity. *Neuron.* **82**, 1367-1379 (2014).
25. G. P. Krishnan, S. Chauvette, I. Shamie, S. Soltani, I. Timofeev, S. S. Cash, E. Halgren, M. Bazhenov, Cellular and neurochemical basis of sleep stages in the thalamocortical network. *Elife.* **5**, (2016).
26. M. Biel, C. Wahl-Schott, S. Michalakis, X. Zong, Hyperpolarization-activated cation channels: from genes to function. *Physiological Reviews.* **89**, 847-885 (2009).
27. S. Ray, N. E. Crone, E. Niebur, P. J. Franaszczuk, S. S. Hsiao, Neural correlates of high-gamma oscillations (60-200 Hz) in macaque local field potentials and their potential implications in electrocorticography. *Journal of Neuroscience.* **28**, 11526-11536 (2008).
28. N. Kraus, T. Nicol, in *Encyclopedia of Neuroscience,* M. Binder, N. Hirokawa, U. Windhorst, Eds. (Springer Berlin Heidelberg, 2009), chap. 433, pp. 214-218.
29. I. Timofeev, M. Steriade, Low-frequency rhythms in the thalamus of intact-cortex and decorticated cats. *Journal of Neurophysiology.* **76**, 4152-4168 (1996).
30. M. Steriade, Grouping of brain rhythms in corticothalamic systems. *Neuroscience.* **137**, 1087-1106 (2006).
31. Y. Nir, R. J. Staba, T. Andrillon, V. V. Vyazovskiy, C. Cirelli, I. Fried, G. Tononi, Regional slow waves and spindles in human sleep. *Neuron.* **70**, 153-169 (2011).
32. A. Crespel, P. Coubes, M. Baldy-Moulinier, Sleep influence on seizures and epilepsy effects on sleep in partial frontal and temporal lobe epilepsies. *Clin Neurophysiol.* **111 Suppl 2**, S54-59 (2000).
33. L. Marshall, H. Helgadottir, M. Molle, J. Born, Boosting slow oscillations during sleep potentiates memory. *Nature.* **444**, 610-613 (2006).
34. S. C. Mednick, E. A. McDevitt, J. K. Walsh, E. Wamsley, M. Paulus, J. C. Kanady, S. P. Drummond, The critical role of sleep spindles in hippocampal-dependent memory: a pharmacology study. *Journal of Neuroscience.* **33**, 4494-4504 (2013).
35. R. Huber, M. F. Ghilardi, M. Massimini, G. Tononi, Local sleep and learning. *Nature.* **430**, 78-81 (2004).
36. B. Rasch, J. Born, About sleep's role in memory. *Physiological Reviews.* **93**, 681-766 (2013).
37. D. Ji, M. A. Wilson, Coordinated memory replay in the visual cortex and hippocampus during sleep. *Nature Neuroscience.* **10**, 100-107 (2007).
38. A. Sirota, J. Csicsvari, D. Buhl, G. Buzsaki, Communication between neocortex and hippocampus during sleep in rodents. *Proc Natl Acad Sci U S A.* **100**, 2065-2069 (2003).
39. M. Steriade, I. Timofeev, F. Grenier, Natural waking and sleep states: a view from inside neocortical neurons. *Journal of Neurophysiology.* **85**, 1969-1985 (2001).
40. J. Talairach, P. Tournoux, *Co-planar stereotaxic atlas of the human brain: 3-dimensional proportional system: an approach to cerebral imaging*. (Thieme, Stuttgart, Germany, 1998).
41. H. Duvernoy, *The Human Brain: Surface, Blood Supply, and Three-Dimensional Sectional Anatomy*. (Springer, ed. 2nd, 1999).
42. A. Morel, M. Magnin, D. Jeanmonod, Multiarchitectonic and stereotactic atlas of the human thalamus. *Journal of Comparative Neurology.* **387**, 588-630 (1997).

43. B. A. Riedner, V. V. Vyazovskiy, R. Huber, M. Massimini, S. Esser, M. Murphy, G. Tononi, Sleep homeostasis and cortical synchronization: III. A high-density EEG study of sleep slow waves in humans. *Sleep.* **30**, 1643-1657 (2007).
44. M. Ushimaru, Y. Ueta, Y. Kawaguchi, Differentiated participation of thalamocortical subnetworks in slow/spindle waves and desynchronization. *Journal of Neuroscience.* **32**, 1730-1746 (2012).
45. V. Crunelli, M. L. Lorincz, A. C. Errington, S. W. Hughes, Activity of cortical and thalamic neurons during the slow (<1 Hz) rhythm in the mouse in vivo. *Pflugers Arch.* **463**, 73-88 (2012).
46. M. Kutner, C. Nachtsheim, J. Neter. (McGraw Hill Education, 2004).
47. R. R. Hocking, A Biometrics Invited Paper. The Analysis and Selection of Variables in Linear Regression. *Biometrics.* **32**, 1-49 (1976).
48. P. C. Austin, J. V. Tu, Bootstrap Methods for Developing Predictive Models. *The American Statistician.* **58**, 131-137 (2004).
49. R Development Core Team. (R Foundation for Statistical Computing, Vienne, Austria, 2004).
50. MATLAB, *version 8.3.0.532 (R2014a).* (The MathWorks Inc., 2014).
51. A. Delorme, S. Makeig, EEGLAB: an open source toolbox for analysis of single-trial EEG dynamics including independent component analysis. *Journal of Neuroscience Methods.* **134**, 9-21 (2004).

Acknowledgements:

The authors wish to thank Donald Hagler for his spindle detection scripts; Fabrice Bartolomei for access to data and analysis input; Catherine Liégeois-Chauvel for research access; Jean Régis for electrode localization for the Marseille patient; Qianqian Deng for analysis assistance; and Maxim Bazhenov, Terry Sejnowski, Jean-Marc Fellous, Giri Krishnan, and Gio Piantoni for scientific discussion. Supported by NIH grants R01-MH099645, R01-EB009282, T32HL07713, ONR grant N00014-13-1-0672, NSF GRFP, and Chateaubriand Fellowship.

Author contributions:

R.M.M., M.R., A.S., C.G., M.R. and H.B. analyzed data. R.M.M., M.R., and A.S. performed statistical analyses. R.M.M., M.M., P.C., M.R., H.B., and E.H. interpreted data and discussed results. R.M.M. and E.H. wrote the manuscript.

Competing financial interests:

The authors report no conflict of interest.

Materials & Correspondence:

Correspondence may be addressed to Eric Halgren (ehalgren@ucsd.edu).

Methods

Recordings

Stereoencephalography (SEEG) was performed on 16 patients with pharmaco-resistant epilepsy at Neurological Hospital, Lyon, France or La Timone Hospital, Marseille, France; however, the recordings of 13 patients were excluded, while the recordings of 3 patients (2 women, 1 man, age: 40.7±8.1) were included for further analysis (Table 1). The recordings of the 13 patients were excluded for the following reasons: the thalamic leads were implicated in the subject's epilepsy (1); the patient had already had tissue resected (1); the thalamic leads were contaminated by artifact (2), there was breakthrough REM activity in the thalamus (2); or there were no useable cortical leads (7).

Subject	Gender	Age	Clinical Diagnosis	Pathological Diagnosis	Imaging	Focus
Sub1	M	35	Right temporal lobe epilepsy	No pathology obtained	Normal	Temporo-Parieto-Occipital Junction
Sub2	F	37	Temporal lobe epilepsy	No pathology obtained	Normal	Hippocampus
Sub3	F	50	Right temporal occipital epilepsy	No pathology obtained	Normal	Right fusiform gyrus

Table 1.
Patient demographics and clinical information.

Fully informed consent was obtained at both hospitals prior to surgery. The ethics committee of Comité Consultatifs de Protection des Personnes se Prêtant à des Recherches Biomédicales Lyon-Centre Léon Bérard and the Institutional Review Board of the French Institute of Health approved these studies. SEEG recording electrodes were implanted according to the stereotactic technique of Talairach and Bancaud to define the epileptogenic area for possible resection. The thalamus was a target of implantation due to its potential role in epileptic discharges. An electrode sampling thalamic areas also had contacts sampling temporal neocortical sites, therefore not increasing patient risk by requiring a separate electrode track.

At both hospitals, each electrode had either 10 or 15 contacts. Each contact was 2mm long, with a diameter of 0.8mm and an inter-contact spacing of 1.5mm.

At the Neurological Hospital, electrodes were perpendicular to the midsagittal plane. The recordings were sampled at 256Hz and band pass filtered from 0.33 to 128Hz. The 3D location of electrode contacts was determined directly from stereotactic teleradiographs without parallax performed within the stereotactic frame (*40*). These locations were superimposed onto the preimplantation 3T structural MRI (3D MPRAGE T1 sequence) after alignment with the skull. The locations of cortical and thalamic contacts were determined by reference to the atlases of (*41*) and (*42*). In Fig. 1d, thalamic nuclei are overlaid on each subject's MRI based on horizontal sections at the indicated distance dorsal to the intercommissural plane from the atlas of (*42*) (Subject 1 in blue and Subject 2 in red).

At La Timone Hospital, the recordings were sampled at 1024Hz and band pass filtered from 0.16 to 340Hz. Electrodes were localized by fusing the CT with electrodes implanted and the MRI (Fig. 1d, Subject 3 is in white).

All analyses were performed on bipolar channels derived from subtracting the lateral lead from the medial lead of two adjacent contacts along an SEEG electrode (Fig. 1e). Bipolar channels included for analysis met both physiological and anatomical criteria as described in (*20*). Only channels exhibiting both slow waves and spindles were included for analysis. Included channels were not part of the epileptogenic focus and did not show frequent epileptiform activity (spikes) or other evidence of damage (pathological slowing). Additionally, times in which brief epileptiform activity occurred were excluded from training data sets and post hoc from any slow wave or spindle detections. A total of 22 cortical and eight thalamic bipolar channels were analyzed. Sleep staging was performed using the bipolar contacts by a qualified rater (MR) and all reported analyses were confined to NREM stages 2 (N2) and 3 (N3).

Downstate detection

Slow waves in cortical and thalamic bipolar channels were detected using a method modified from (*43*) in order to accurately and maximally identify slow waves in the thalamus. A zero-phase fourth order Butterworth bandpass filter from 0.1 to 4Hz was applied to each channel over N2 and N3 periods of sleep that were free of epileptic activity. Consecutive zero crossings occurring within 0.25 to 3 seconds were then selected. The amplitude of the peak between these zero crossings was calculated and only the top and bottom 40% of peaks were retained as slow waves. Downstates and upstates in the cortex were defined based on changes in high gamma power (60-100Hz), with downstates associated with a decrease in high gamma power around the downstate peak and upstates associated with an increase in high gamma power at the time of the upstate peak. This criterion was confirmed by the fact that the downstate is always negative in pial minus white matter trans-cortical bipolar derivations (*20, 23*).

For supplemental analyses, stricter downstate detection parameters were also implemented, whereby consecutive zero crossings were selected between 0.25 to 1secs and the bottom 20% of peaks were retained as downstates (Supplementary Figures 10 & 11).

Unlike cortex, thalamic bipolar recordings have no pre-defined consistent relationship between local slow wave generator polarity and anatomical location. Thus, we initially used broadband power increases to tentatively determine the local bipolar polarities corresponding to downstates and upstates. In Subjects 1 and 2, this determination was confounded by the strong effect of spindles which accounted for most or all of the high gamma increase (Fig. 2 & Supplementary Figures 1 & 4). However, in Subject 3 the wider bandwidth recordings allowed activity in higher frequencies to be measured, and this allowed us to confirm the assignment by showing that the high gamma increase was also present in the absence of spindles (Fig. 6). Subject 3 was sampled at 1024Hz and therefore could be analysed in the high gamma range above 100Hz. First, thalamic slow wave peaks were identified in the 0.1-4Hz bandpassed data. Then the polarity transitions associated with increasing spindling and gamma power were tentatively labelled as down-to-upstate transitions. The peak Hilbert amplitude was calculated on the 10-16Hz bandpassed signal from 0 to 500ms after each putative downstate peak. The downstates were then sorted based on these peak spindle-band amplitudes. The top 10% of spindle-band amplitudes were strongly associated with high gamma power increases during the transition from the downstate to the upstate (Fig. 6A). The bottom 10% did not show any increases in spindle-band power; however, there was still an increase in high gamma power

during the transition from the downstate to the upstate (Fig. 6B). Note that in this approach, we focused on high gamma increases to define the termination of the downstate, rather than the decreases of high gamma as in the cortex. This was necessary because there is very limited baseline high gamma activity in the thalamus, consistent with limited observations in rats (*24*).

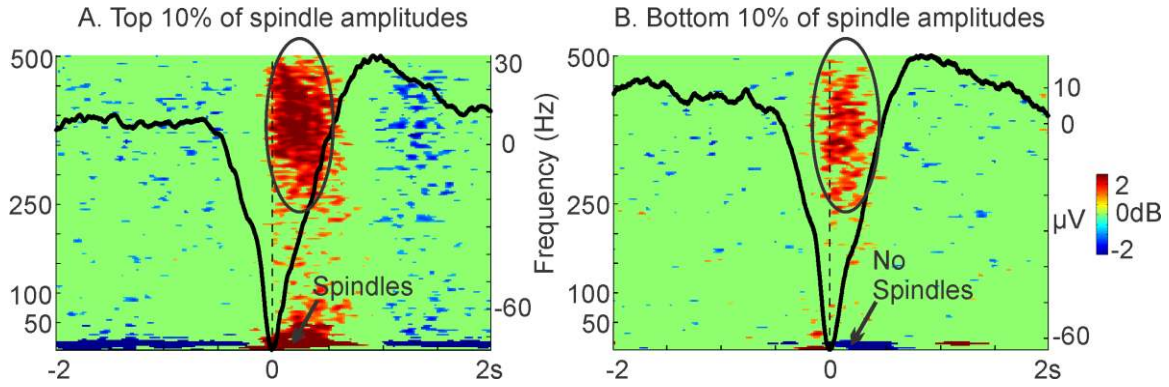

Figure 6. High gamma power changes occur in the thalamus in relation to downstates free of spindles. Downstates detected in the medial pulvinar/lateral pulvinar channel of Subject 3 were sorted based on spindle-band amplitudes. The spindle-band amplitude was measured by taking the maximum of the Hilbert amplitude between 0 to 500ms (downstate peak at 0ms) calculated after applying a 10-16Hz bandpass filter. A. The downstates corresponding to the top 10% of spindle-band amplitudes show a significant increase in both spindle-band and high gamma power. B. The downstates corresponding to the bottom 10% of spindle-band amplitudes do not show a significant spindle-band increase, but do continue to show a significant increase in high gamma power. For both A and B, downstates were epoched from -2.3 to 2.3 seconds around the downstate peaks at 0ms. Time frequency plots are from 5 to 500Hz and baseline corrected over the entire epoch. Significance level was set to $p<0.01$, uncorrected. Waveforms show the averaged local field potential for the same trials.

Additionally, we examined high gamma changes as they related to spindle starts and ends in Subject 3 and found that high gamma decreases are associated with the end of spindles, rather than downstates (Supplementary Figure 1). We therefore concluded that our definition of downstates in the thalamus was valid; unlike cortical high gamma, thalamic high gamma increases occur at the transition from downstates to upstates. Note that our definition of the thalamic downstate, based on high gamma power, is consistent with thalamic and cortical recordings in anaesthetized cats which found, using LFP and intracellular recordings, that rebound firing after a downstate can occur on the down-to-upstate transition, earlier in the thalamus than the cortex (*10*). Recordings in anaesthetized rats also find that in some thalamic nuclei, the slow wave-related firing increases at the down-to-upstate transition (*44*). Recordings in anaesthetized mice further show that rebound burst firing in the thalamus occurs during the transition from hyperpolarization (*45*).

In order to use comparable measures across subjects, analyses performed in all three subjects only examine high gamma up to 100Hz. Only cortical and thalamic downstates were used for further analysis. Post downstate detection artifact rejection was applied to each channel. The difference in consecutive points was calculated to detect any sharp artifacts in the signal and a threshold was set for each channel individually based on visual inspection. Additionally, the

raw data were epoched ± 3seconds around the downstate peaks for each channel. The mean and standard deviation were calculated on the absolute value of this raw epoched data. Thresholds for rejection were evaluated visually for each channel. For all but two channels, a threshold of 7SD was applied. For Subject 1, a rejection threshold was set to 10SD for one middle frontal gyrus channel and a rejection threshold was set to 9SD for a second middle frontal gyrus channel. Within channel, if an artifact occurred within an epoch, then that slow wave was rejected.

Previous spindle detection method

Spindles in cortical and thalamic bipolar channels were detected using a method adapted from that described in (*31*). The N2 and N3 data for each channel were bandpass filtered using a zero-phase fourth order Butterworth filter from 10-16Hz. The mean of the Hilbert envelope smoothed with a gaussian kernel (300ms window; 40ms sigma) was calculated on this band passed signal for each channel. The spindle detection threshold was set at mean +3SD, with the start and stop set at mean +1SD. We lowered the length required for a spindle from 0.5 seconds to 0.3 seconds, while maintaining the upper bound of 2 seconds.

We found, however, that a large number of spindles in the thalamus were not detected using this method. To account for thalamic channels being much smaller in amplitude than cortical channels, and for thalamic channels being largely dominated by spindle activity, we modified the above detection parameters: the spindle detection threshold was lowered to mean +1.5 SD, while maintaining the mean +1 SD for the start and stop for the thalamic channels. Undetected thalamic spindles still remained clearly discernible in the raw data. Therefore, the spindle detection method described below was developed in order to robustly detect spindles using the same method in both cortical and thalamic channels.

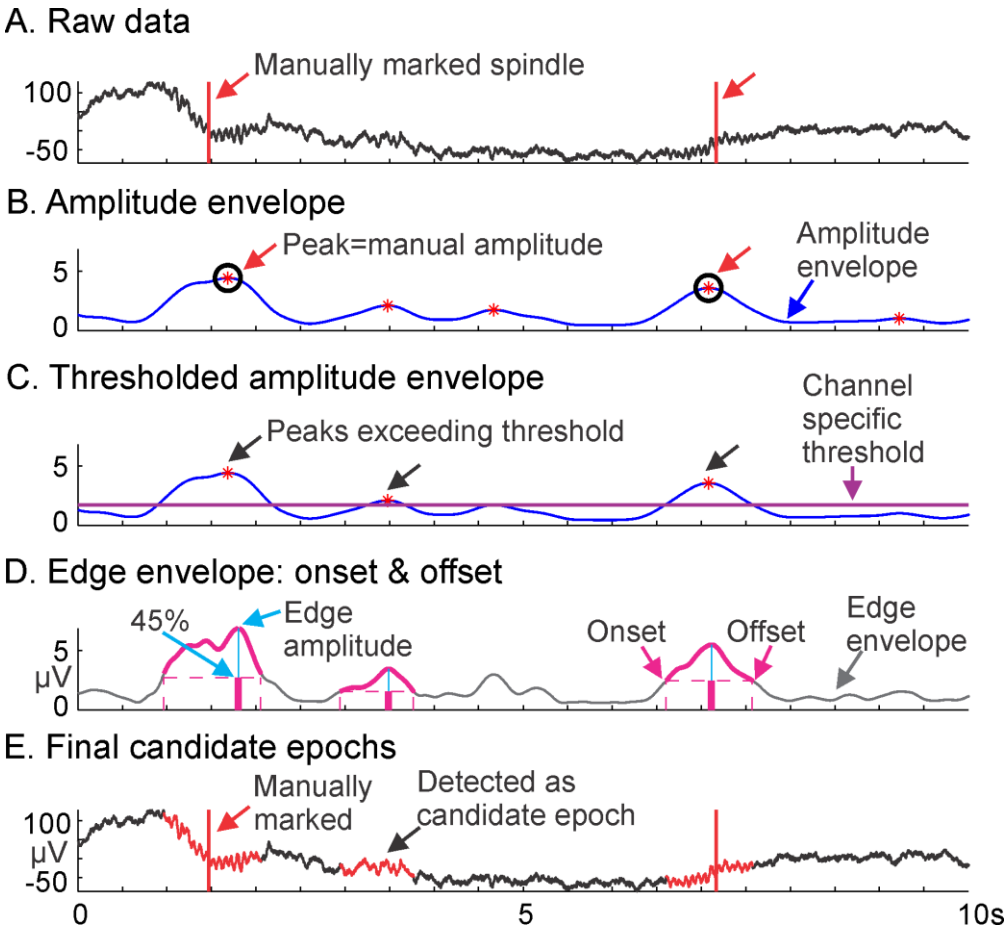

Figure 7. Selection of candidate epochs by current spindle detection method. A. Spindles are manually marked (red lines) on 10 minutes of N2 and 10 minutes of N3 raw data, per channel. B. The amplitude of peaks in the amplitude envelope corresponding to manually marked spindles are calculated (manual amplitude, black circles). C. A per channel threshold (purple line) is applied to the amplitude envelope based on the lowest manual amplitude for that channel. Peaks, marked by red asterisks, which exceed that threshold are kept as candidate epochs. D. The closest peak in the edge envelope to the selected peak in the amplitude envelope is detected as the edge amplitude (blue vertical lines). The bounds of the onset and offset of the spindle (pink traces) are calculated at 45% or greater of this edge amplitude. E. The final candidate epochs highlighted in red include epochs where spindles had (red lines) and had not (black arrow) been manually marked.

Current spindle detection method

To begin, individual spindles were exhaustively marked on each channel for 10 minutes of N2 sleep and 10 minutes of N3 sleep per subject (marked by R.M.M., Fig. 7a). Spindles over the whole dataset for each subject were then detected in two steps. In the first step, potential spindles are automatically selected; these are the candidate epochs. In the second step, a decision as to whether these candidate epochs are spindles or not was performed using a logistic regression.

In the first step of spindle detection, to define the candidate epochs, a 10-16Hz bandpass was applied to the data and the absolute value of the band passed signal was taken. The resulting signal was convolved with an average Tukey window of 400ms. This envelope (the edge envelope) was used to define the onset and offset of the candidate epochs (Fig. 7d). A second

convolution between the edge envelope and a 600ms average Tukey window was applied. This envelope (the amplitude envelope) was used to locate the candidate epochs (Fig. 7b).

All peaks in this amplitude envelope where spindles had been manually marked were found (Fig. 7b). These were considered the manual amplitudes. For each channel, the smallest of these manual amplitudes was used as the candidate epoch threshold for that channel. Candidate epochs were therefore located at each peak in the amplitude envelope greater than this smallest manual amplitude for that channel (Fig. 7c). For each of these peaks in the amplitude envelope, the amplitude of the closest peak in the edge envelope was found and considered the edge amplitude. The onset and offset for the candidate epoch was defined as periods where the edge envelope was greater than or equal to 0.45*the edge amplitude (Fig. 7d). All candidate epochs shorter than 300ms were discarded. Final candidate epochs included epochs where spindles had and had not been manually marked (Fig. 7e).

In the second step of spindle detection, a set of metrics was computed for each candidate epoch. The spindle amplitude (Amp) was the maximum amplitude of the amplitude envelope within the epoch. Dur was the duration of the spindle equal to onset – offset. The spindle_power was the maximum amplitude of the FFT of the signal between 10-16Hz. The nonspindle_power was the maximum amplitude of the FFT of the signal between 5-8 Hz. The F_ratio was the ratio: Spindle_power/Nonspindle_power. The spindle_freq was the frequency where the FFT in the 10-16Hz range is maximal. The sband_amp was the max of the edge envelope between onset and offset. Similar to the edge envelope, we computed the low band envelope between 4-8Hz and the high band envelope from 18-25Hz. Lband_amp is the maximum of the low band envelope between onset and offset. Hband_amp is the maximum of the high band power between onset and offset. Stage was the sleep stage. Npeaks was the number of peaks of the spindle. Peakrate is the ratio: npeaks/dur. Peak_intv_mean and peak_intv_std are the peak interval mean and standard deviation. Pr is a binary variable indicating whether peakrate is within spindle range or not.

Using these metrics and the marked periods of data, a logistic regression was used to determine which candidate epochs were spindles. Spindle events (1) were all candidate epochs marked as spindles. Non-spindle events (0) were all candidate epochs within the marked periods of time not marked as spindles (Fig. 7e). Because of the observed discrepancies between channels, a model was developed for each channel.

To quantify the correlation between each of our metrics that could cause multicollinearity issues in the stepwise selection, the generalized Variance Inflation Factors (VIF) (*46*) for each predictor in the complete model were computed. As in (*46*) if the VIF for the predictor with the maximum VIF was greater than 10, this predictor was removed. The step was repeated until no selected predictor had a VIF greater than 10. Once all variables that are not too highly correlated were selected, a bidirectional stepwise selection was applied to select a model (*47*) with all the variables that best explain the spindle events. A bootstrap analysis was then performed to ensure that the model selection was stable (*48*).

The logistic regression was trained on the marked data and we calculated the probability of each candidate epoch over the whole dataset being a spindle. To determine the probability threshold above which a candidate epoch was considered a spindle, the number of False Positives (FP), False Negatives (FN), True Positives (TP) and True Negatives (TN) were computed, for multiple thresholds between 0% and 100% using a leave one out cross validation method. The final threshold was the probability that minimized the difference between the False Positive Rate (FPR) and the False Negative Rate (FNR), where FPR = FP/(FP+FN) and FNR =

FN/(TP+FN). Analyses were performed using the *glm* procedure, the *vif* procedure of the "car" package, the *stepAIC* of the "MASS" package and the *boot.stepAIC* procedure of the "bootStepAIC" package of the R software (*49*).

Periods in which epileptic activity occurred were not used for marking spindles. Spindles that occurred during epileptic times or outside of N2/N3 were eliminated *post hoc*. In addition, *post hoc* artifact rejection as described for slow waves above was applied to spindles, except that the data were epoched from -2 to 4 seconds around the start of the spindle before calculating the artifact rejection standard deviation threshold and subsequently rejecting epochs.

To determine how well the spindle method described above and the spindle method described in (*31*) performed, we compared the spindles detected by each method to the manually-detected spindles in the 10 minutes of N2 and 10 minutes of N3 in each channel (Supplementary Table 1). In applying the method described in (*31*) to our data, we set the threshold for cortical channels to mean +3SD and the threshold for thalamic channels to mean +1.5SD. We also lowered the spindle duration to 0.3 seconds to match the duration requirements set in our current detection method. For testing of our method, these numbers were calculated using cross-validation. For each method, the number of true positives (manually marked as a spindle, predicted as a spindle), false positives (not manually marked as a spindle, but predicted as a spindle), and false negatives (manually marked as a spindle, but not predicted as a spindle) were calculated for each channel and averaged over cortical channels and thalamic channels for each subject.

We found that in this dataset our spindle detection method outperformed the traditional detection method outlined in (*31*), with a greater number of true positives and substantially fewer false negatives (Supplementary Table 1). Our spindle detection method also had a lower number of false positives for the thalamic channels in all subjects, but a higher false positive rate in the cortex, compared with the previous method. Our hit rate was higher in all cases. Due to the higher number of false positives in our cortical detections, the false alarm rate was also higher for all subjects in the cortical channels. The d' measure indicates how well each detection method discriminated between spindles and non-spindles. The d' value was higher in both the cortex and thalamus for all subjects with our current method compared to the previous method. As shown in Supplementary Table 1, d' in the cortex was .73 vs. 1.82, 1.15 vs. 1.85, and 1.25 vs. 1.45, comparing the Previous vs. Current method in subjects 1, 2 and 3. Similarly, d' in the thalamus was 1.05 vs. 1.90, 1.52 vs. 2.18, and 1.19 vs. 1.90, comparing the Previous vs. Current method in subjects 1, 2 and 3. C measures the bias towards false positives or false negatives. In all cases, except for in the cortex for subject 3, the bias was in the same direction for both detection methods. Again, except for in the cortex for subject 3, C was smaller for the current detection method compared to the previous method. In sum, these measures indicate that our current detection method discriminated spindles more accurately and with less bias than the previous method, for our dataset.

Analyses

Histograms of the number of events in 50ms time bins were calculated locking to either downstate peaks or spindle starts and examining the timing of downstate peaks, spindle starts, or spindle ends within or across channels. For example, a histogram height of 10 (on the y-axis) in the -300 to -350ms bin (on the x-axis) in the insula versus pulvinar downstate plot would mean that the peaks of 10 downstates in the insula channel occurred between 300 and 350ms before a downstate in the indicated pulvinar channel.

Binomial tests of the null hypothesis of random temporal order were performed on the number of downstate peaks or spindle starts occurring in one temporal order versus the reverse temporal order for each corticothalamic channel pair over ±500ms. For slow waves occurring at ~1Hz, this time limit was chosen to limit the possibility of false detections (i.e., detecting a slow wave from another cycle in the paired channel). Bonferroni correction was applied at $p<0.05$ over all thalamocortical pairs, separately for downstates and spindles, which resulted in a significance level of $p<0.00078$.

The average delay from cortical downstate peak to thalamic downstate peak was calculated on corticothalamic pairs significant for the binomial test described above in the cortical to thalamic direction. For each of these 28 pairs, only downstate events in which a cortical downstate occurred within 500ms before a thalamic downstate occurred were used. Locking to the times of the thalamic downstate peaks for these overlapping events, the average 0.1 to 4Hz bandpassed cortical downstate waveform was calculated. The latency for each corticothalamic pair was then determined by the time of the minimum peak in the cortical downstate wave. The overall average latency was calculated by averaging over each of these corticothalamic pairs.

The average delay from downstate onset to spindle onset in the thalamus was calculated on the downstate waveforms and spindle histograms plotted in Fig. 2b & Supplementary Figure 4, left columns. Downstate onset was determined on the averaged 0.1 to 4Hz bandpassed downstate for each thalamic channel. A 20^{th} order polynomial was fit to this average waveform before calculating the polynomial's second derivatives (i.e. inflection points). The inflection point closest to the visually-determined downstate onset was recorded for each thalamic channel. Spindle onset was determined by choosing the latency (middle of the 50ms bin) corresponding to the spindle peak in each histogram. The average delay for each thalamic channel was calculated by subtracting the spindle onset time from the downstate onset.

In order to determine the relationship of gamma to individual spindle peaks in Figure 3e, gamma was calculated by taking the analytic amplitude from the Hilbert transform of the data filtered from 55 to 100Hz using a zero-phase fourth order Butterworth filter. A spline interpolation was applied to the gamma before calculating the time between the gamma peaks in the thalamic and cortical channels. This delay in gamma peak times was used to measure the average delay from thalamic to cortical spindles.

The enrichment factor was calculated to quantify how much more likely an event was to occur in temporal relation with another event. For example, how much more likely spindles were to occur in relation to downstates (DS), compared with the overall spindle density for a channel. The enrichment factor for each channel was the peak spindle-DS density divided by the overall spindle density. The peak spindle-DS density was calculated per channel by taking the number of spindles in the tallest 50ms bin within ± 500ms of the DS peak. This peak spindle-DS density per minute was computed as follows: (20*60*number of spindles in tallest bin)/number of downstates for that channel. The overall spindle density was calculated by dividing the total number of spindles per channel by the total number of minutes of N2/N3 sleep over which spindles were detected. The enrichment factor was also calculated for downstates in one channel compared to downstates in another channel, spindles in one channel compared to spindles in another channel, and spindles in one channel compared to downstates in another channel, as outlined in Supplementary Figure 8. The calculations were derived in the same way, except that the number of events in the tallest bin would be from one channel and the number of events would be from the other channel.

The proportion of spindles occurring with a downstate was calculated to quantify the degree to which spindles are locked to downstates in the thalamus versus the cortex. As cortical spindles arise during the downstate-to-upstate transition, while thalamic spindles arise during the downstate, different time ranges were used for thalamic and cortical channels. For cortical channels, spindles beginning within 750ms after the downstate peak were tabulated, while in thalamic channels, spindles were counted if they began within -500ms to + 250ms of the downstate peak. To account for a larger overall number of downstates in the cortex compared to the thalamus, the normalized proportion of spindles occurring with a downstate was calculated as follows for each channel: (number of spindles occurring with a downstate/total number of spindles)/(total number of downstates/largest total number of downstates within subject).

All analyses were performed in Matlab 2014a (*50*). All time frequency plots were generated using EEGLAB (*51*).

Data availability

The datasets analyzed during the current study are not publicly available due to privacy concerns but are available from the corresponding author on reasonable request.

Code availability

All analyses were performed using Matlab 2014a and R, along with publically available toolboxes, as detailed in the Methods. Code is available from the corresponding author on reasonable request.

Supplementary Information

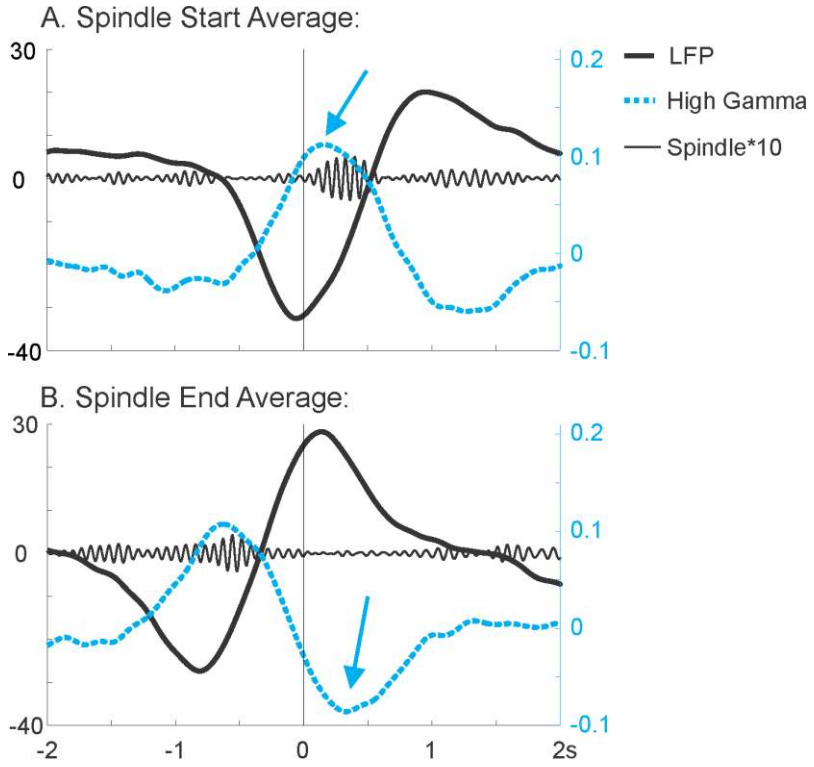

Supplementary Figure 1. High gamma decreases in the thalamus are related to the end of spindles. In Subject 3, the local field potential (0.1 to 4Hz bandpass, thick black line), high gamma amplitude (Hilbert analytic amplitude on data bandpassed from 250 to 500Hz and then bandpassed from 0.1 to 4Hz, blue dotted line), and spindle (10-16Hz bandpass, thin black line) are plotted for the medial pulvinar/lateral pulvinar channel. The spindle trace has been multiplied by 10 for display purposes. Blue arrows indicate the high gamma increases or decreases in each subplot. A. The local field potential (LFP), high gamma amplitude, and spindle locked to the start of spindles. There is a clear high gamma increase after the downstate LFP peak that coincides with the start of spindles. B. The LFP, high gamma amplitude, and spindle locked to the end of spindles. A clear high gamma decrease occurs at the end of spindles.

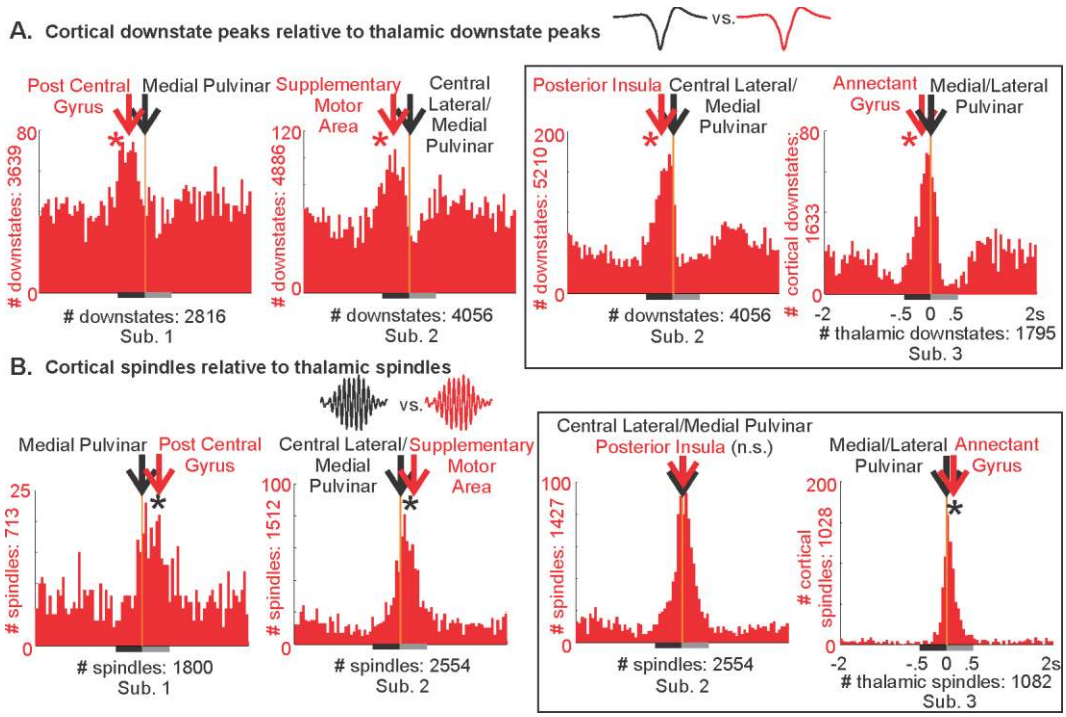

Supplementary Figure 2. Histograms of corticothalamic pairs for downstates and spindles. A. Timing of cortical downstates relative to thalamic downstates: thalamic downstate peaks are locked at 0ms (vertical orange lines) and the corresponding cortical downstate peaks are plotted in red 50ms bins. In all cases, the time of maximal cortical downstate occurrence (red arrow) leads thalamic downstates (black arrow). The number of cortical downstates was significantly more in the 500ms prior to the thalamic downstates, as compared to the 500ms after (*, binomial test, Bonferroni corrected at $p<0.05$; all p-values listed in Supplementary Table 3A). Box indicates relatively strongly connected corticothalamic pairs (see Supplementary Note 2). B. Timing of cortical spindles relative to thalamic spindles: thalamic spindle onsets are locked at 0ms (vertical orange lines) and the corresponding cortical spindle onsets are plotted in red 50ms bins. All pairs are the same as in A. The number of cortical spindles was significantly more in the 500ms after the thalamic spindles, as compared to the 500ms prior (*, binomial test, Bonferroni corrected at $p<0.05$; all p-values listed in Supplementary Table 3B), for all but one pair. In the central lateral/medial pulvinar versus posterior insula (n.s.), the spindles onset nearly simultaneously.

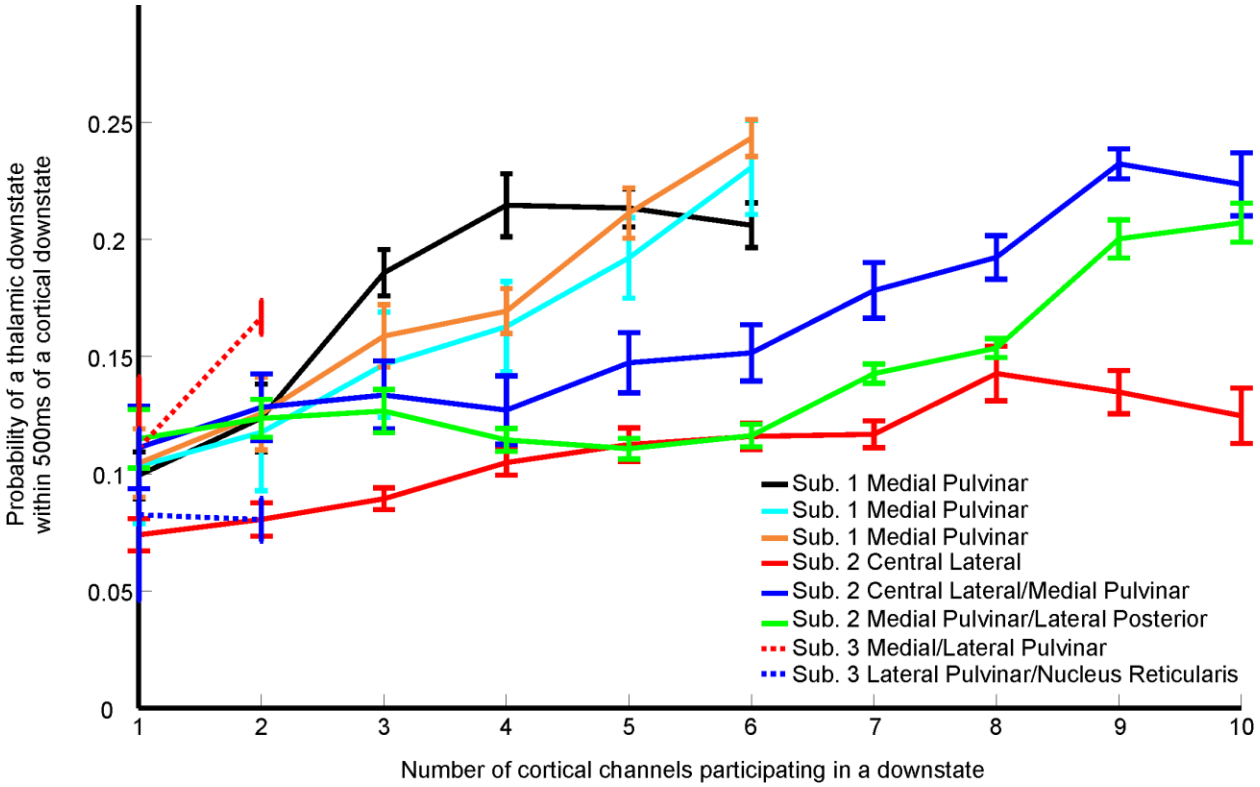

Supplementary Figure 3. The probability of a thalamic downstate increases as the number of cortical channels participating in a cortical downstate increases. For each subject, the number of downstates occurring within 500ms after one other cortical channel, up to the maximum number of cortical channels, was calculated. For each thalamic channel, the probability of thalamic downstates occurring within 500ms after cortical downstates was calculated for all combinations of cortical channels. When a downstate occurred in two or more cortical channels, the downstate peak of the locked cortical channel was used to search for thalamic downstates. Each colored line represents the mean ± SEM for each thalamic channel. In most thalamic channels, as more cortical channels participate in a downstate, the probability of a thalamic downstate increases.

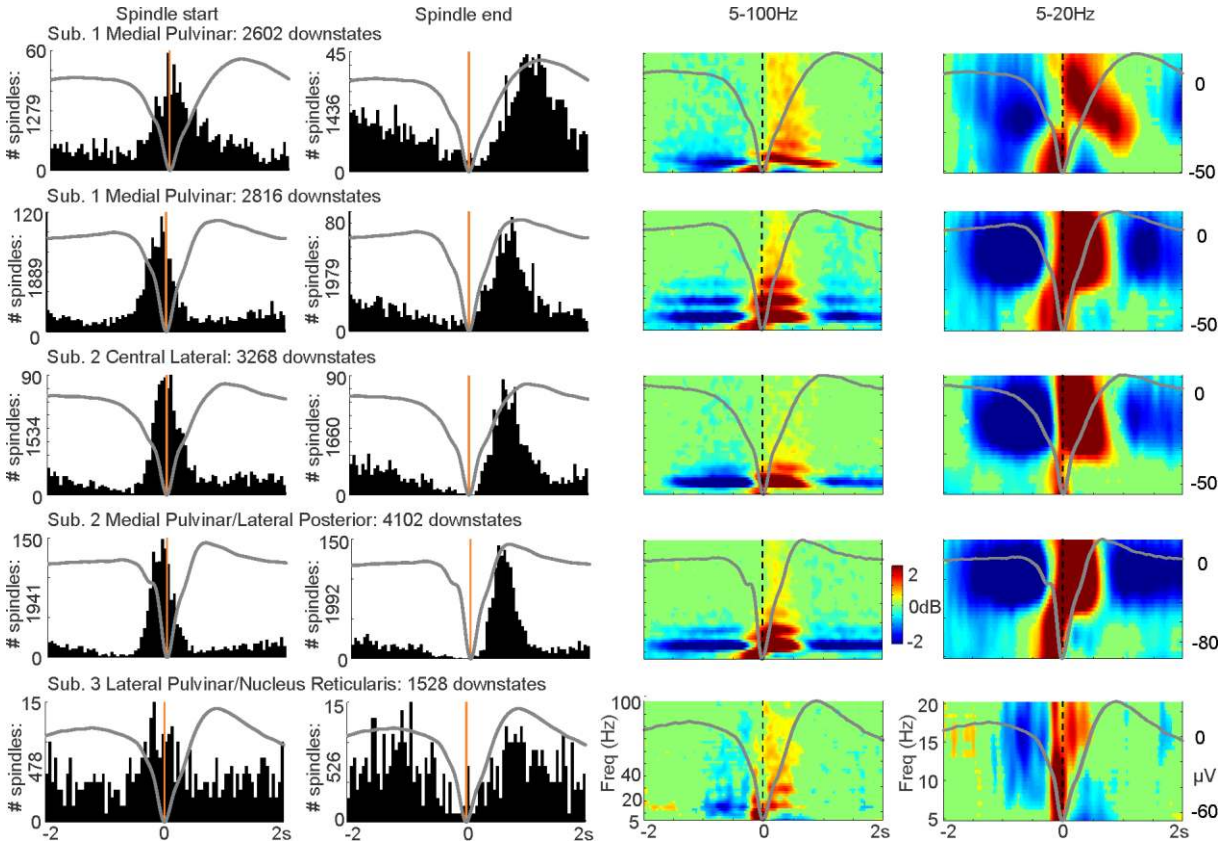

Supplementary Figure 4. On average, spindles start at the thalamic downstate peak, and end at the following thalamic upstate peak. Histograms of thalamic spindle onsets (first column) or spindle terminations (second column) in relation to the thalamic downstate peak at 0ms (orange vertical lines) for each thalamic channel in 50ms bins. Spectral power from 5-100Hz (third column), or from 5-20Hz (fourth column) averaged on the downstate peaks at 0ms, baseline corrected over entire epoch, thresholded at $p<0.01$, uncorrected. Channels plotted here and in Fig. 2B comprise all thalamic channels. Waveforms show the averaged local field potential in each channel.

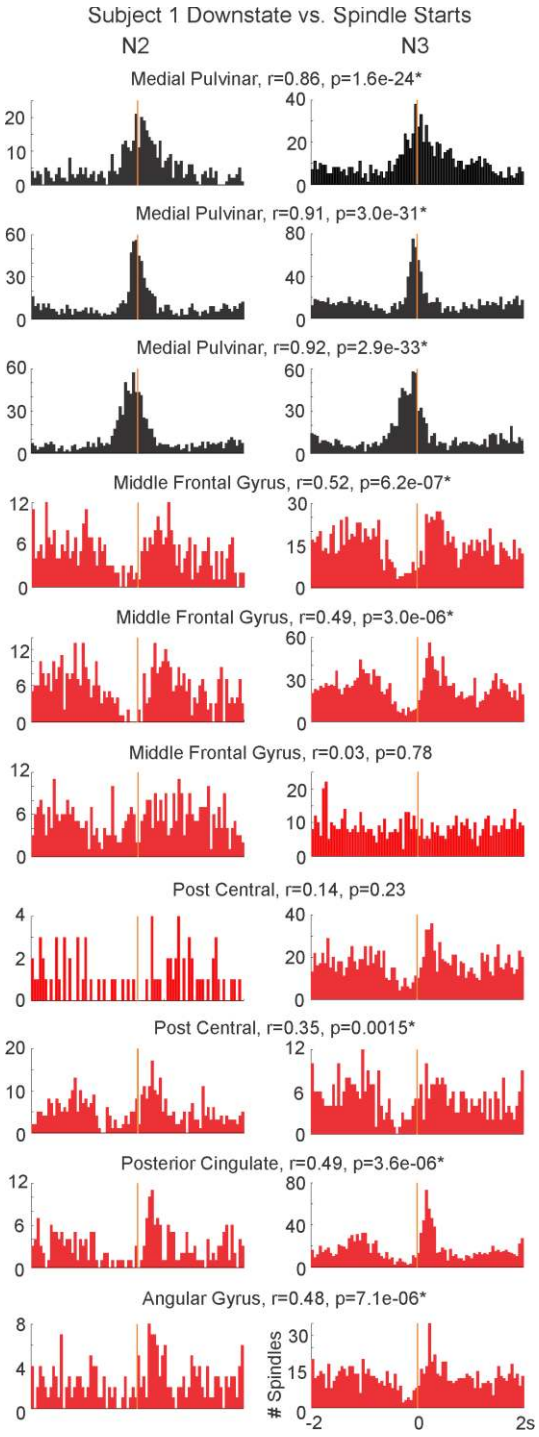

Supplementary Figure 5. Downstate versus spindle relationship in N2 versus N3 for Subject 1. In each row, the spindle starts occurring within ±2 seconds of N2 downstate (left) or N3 downstate (right) peaks are plotted in 50ms bins for each channel. Vertical orange lines mark the local downstate peaks at 0ms for each channel. The overall shape of the spindle distributions locked to downstates appears similar in N2 and N3 for each channel: thalamic spindles occur clustered around the downstate peak (black histograms), while cortical spindles arise after the downstate peak (red histograms). For each channel, the correlation coefficient between N2 and

N3 spindles occurring in relation to downstates was calculated. The location, correlation coefficient, r, and the p-value for the correlation, are calculated for each channel. P-values<0.05, corrected for multiple comparisons, are marked with an asterisk and indicate that the distributions arising in relationship to downstates are significantly correlated between N2 versus N3 spindles. Here, one middle frontal gyrus channel and one post central channel do not have significant correlations; however, the pattern of spindles related to downstates is less clear for this middle frontal gyrus channel than other channels and the number of spindles arising in N2 for this post central channel is small, although they both show a tendency to occur after the downstates.

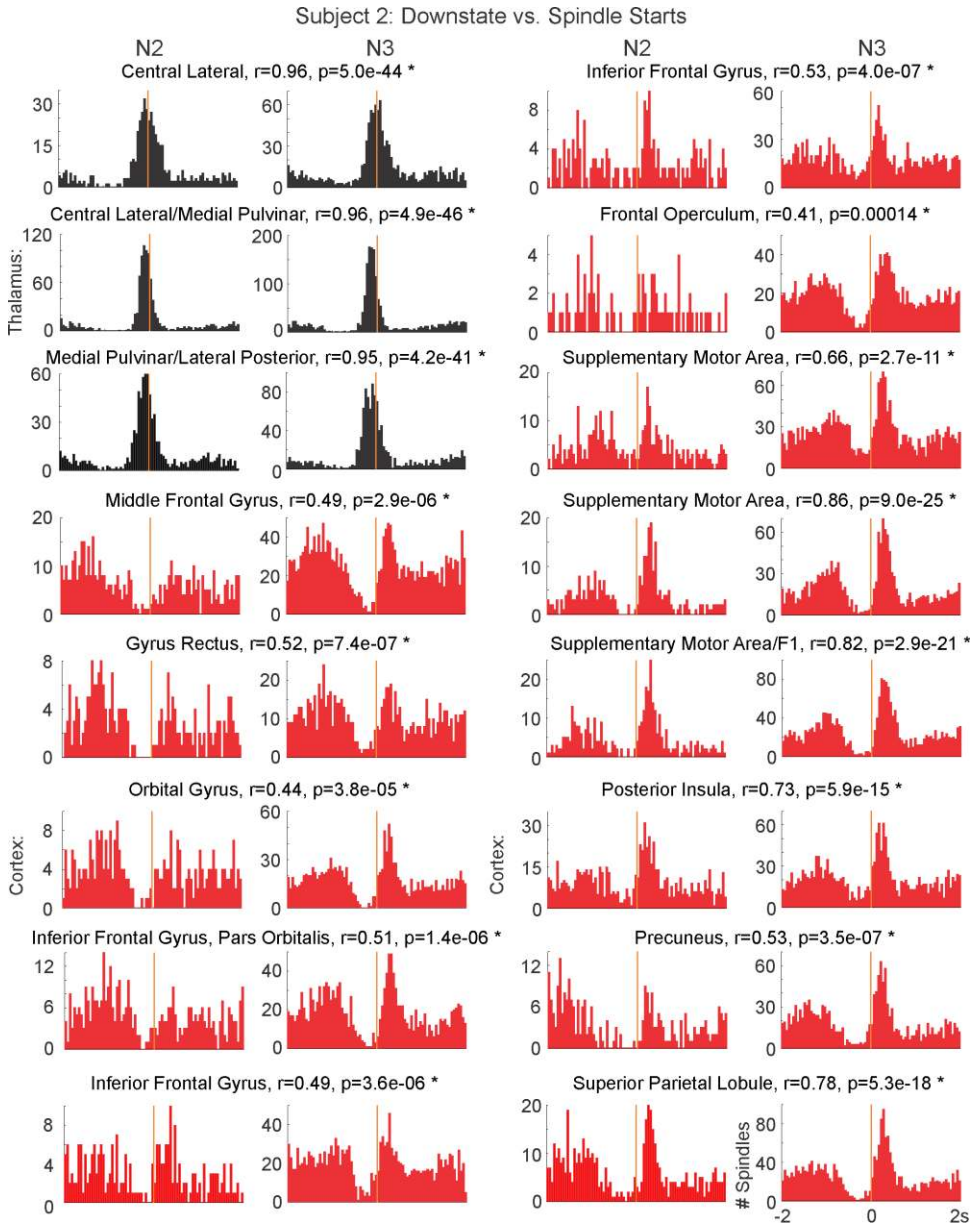

Supplementary Figure 6. **Downstate versus spindle relationship in N2 versus N3 for Subject 2**. The spindle starts occurring within ±2 seconds of N2 downstate (left) or N3 downstate (right) peaks are plotted in 50ms bins for each channel. Vertical orange lines mark the local downstate peaks at 0ms for each channel. The overall shape of the spindle distributions locked to downstates appears similar in N2 and N3 for each channel: thalamic spindles occur clustered around the downstate peak (black histograms), while cortical spindles arise after the downstate peak (red histograms). For each channel, the correlation coefficient between N2 and N3 spindles occurring in relation to downstates was calculated. The location, correlation coefficient, r, and the p-value for the correlation, are calculated for each channel. P-values<0.05, corrected for multiple comparisons, are marked with an asterisk and indicate that the distributions arising in relationship to downstates are significantly correlated between N2 versus N3 spindles. All channels show a significant correlation.

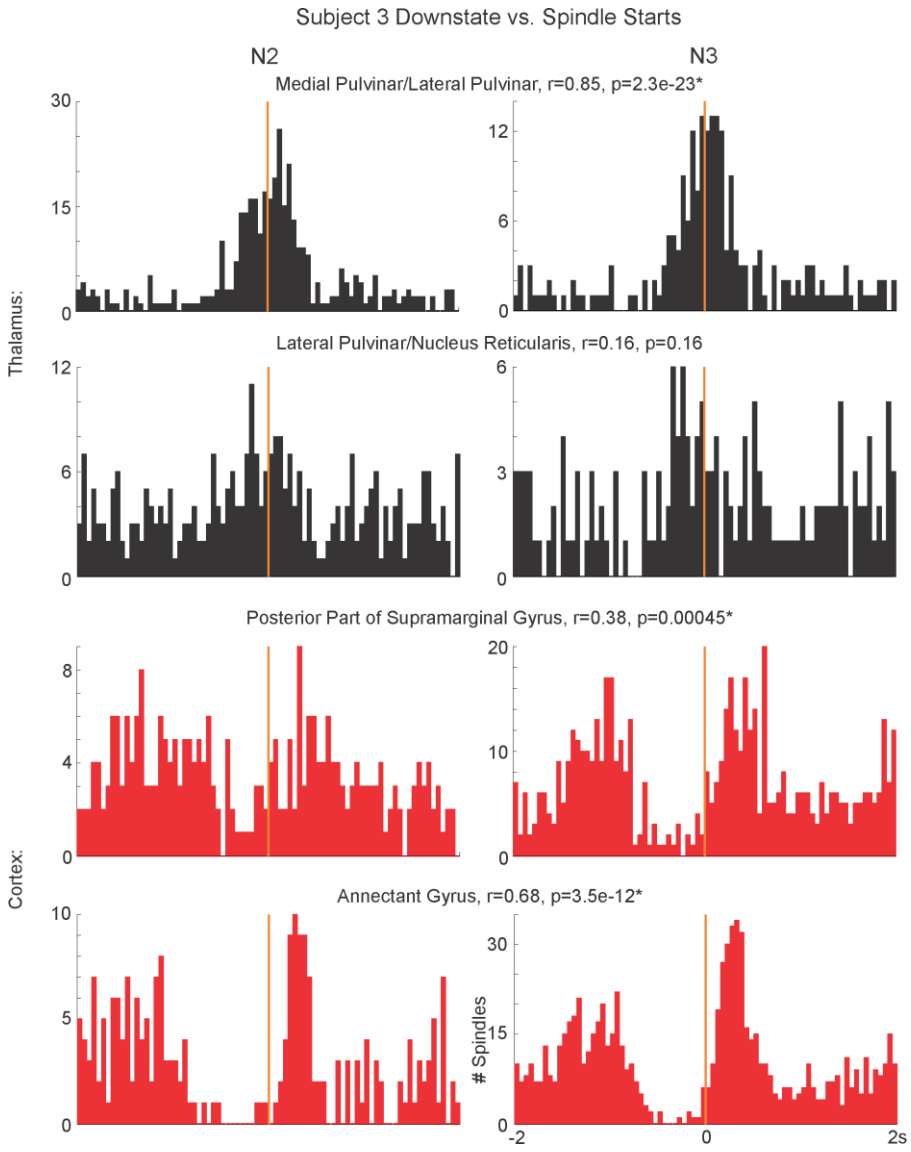

Supplementary Figure 7. **Downstate versus spindle relationship in N2 versus N3 for Subject 3.** The spindle starts occurring within ±2 seconds of N2 downstate (left) or N3 downstate (right) peaks are plotted in 50ms bins for each channel. Vertical orange lines mark the local downstate peaks at 0ms for each channel. The overall shape of the spindle distributions locked to downstates appears similar in N2 and N3 for each channel: thalamic spindles occur clustered around the downstate peak (black histograms), while cortical spindles arise after the downstate peak (red histograms). For each channel, the correlation coefficient between N2 and N3 spindles occurring in relation to downstates was calculated. The location, correlation coefficient, r, and the p-value for the correlation, are calculated for each channel. P-values<0.05, corrected for multiple comparisons, are marked with an asterisk and indicate that the distributions arising in relationship to downstates are significantly correlated between N2 versus N3 spindles. All channels except for the lateral pulvinar/nucleus reticularis have a significant correlation. In this channel, the spindles are still clustered around 0 for N2 and N3, but appear more clustered to the left of 0 in N3.

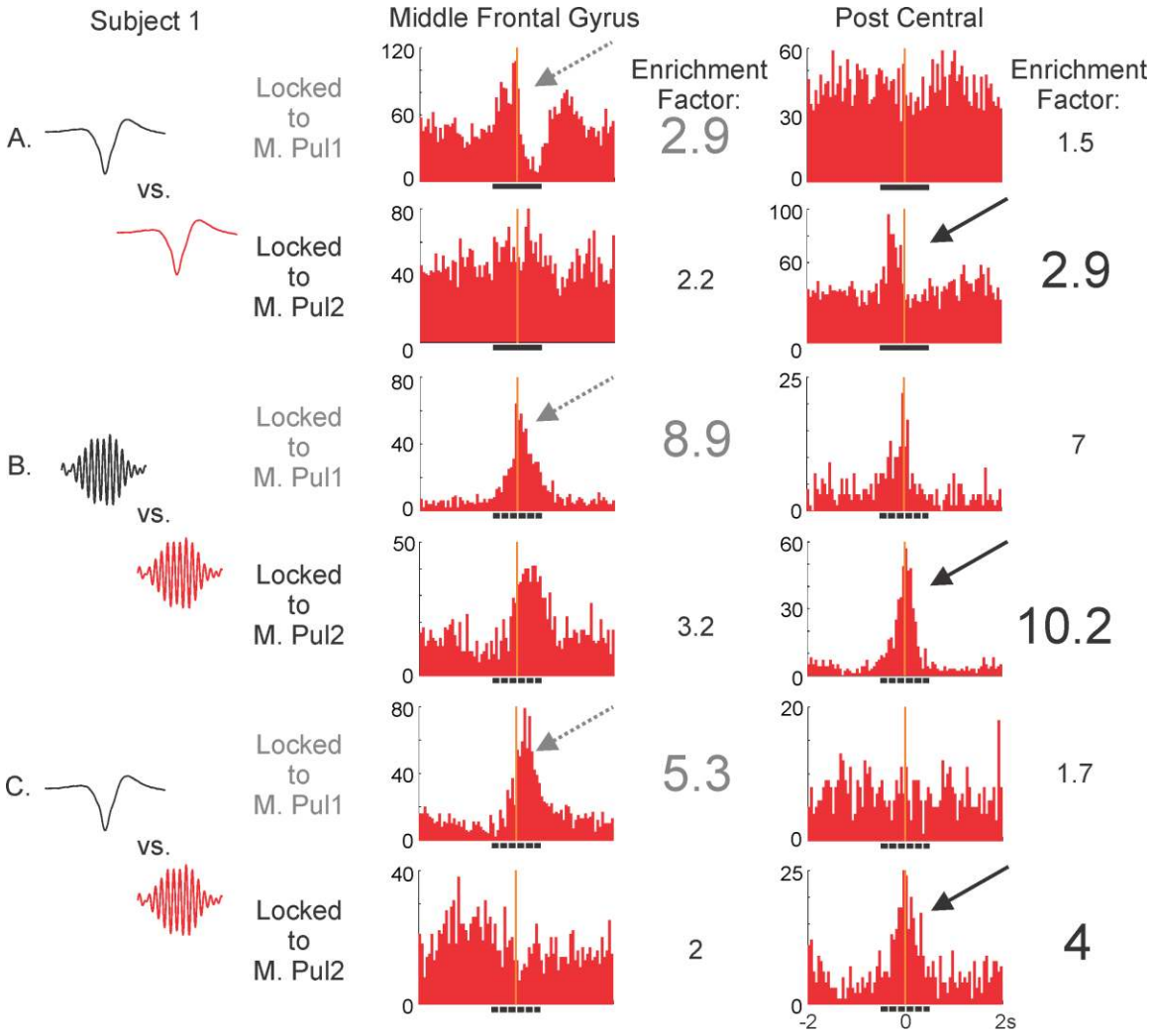

Supplementary Figure 8. Different parts of medial pulvinar are related to different parts of cortex in Subject 1 during downstates and spindles. Events arising in the middle frontal gyrus channel (left column) or the post central channel (right column) are locked to events in the medial pulvinar channels M. Pul1 (labeled in grey) or M. Pul2 (labeled in black). The three event combinations are: downstate versus downstate (A), spindle versus spindle (B), and downstate versus spindle (C). The enrichment factor (see Methods) denotes how the density of downstates or spindles in the cortical channel is increased relative to its normal density when locked to the downstate or spindle events in the medial pulvinar channel. Solid lines (downstates) or dashed lines (spindles) under each histogram denote the ±500ms over which the enrichment factor was calculated. Grey arrows and grey enrichment factors indicate the related M. Pul1/Middle Frontal Gyrus pair. Black arrows and black enrichment factors indicate the related M. Pul2/Post Central pair. A. Downstate versus downstate. Downstates in the Middle Frontal Gyrus peak just before the M. Pul1 downstates at 0ms and drop sharply afterwards. In contrast, Post Central downstates locked to M. Pul1 downstates occur more randomly in time. These patterns reverse when the cortical channels are locked to the second thalamic channel, M. Pul2. The downstate versus downstate enrichment factor is greatest for M. Pul1/ Middle Frontal Gyrus and M. Pul2/ Post Central (2.9 for both), compared to 1.5 for M. Pul1/ Post Central and

2.2 for M. Pul2/ Middle Frontal Gyrus. B. Spindle versus spindle. The highly associated M. Pul1/ Middle Frontal Gyrus and M. Pul2/ Post Central thalamocortical pairings share spindles centered on 0 and both have high enrichment factors (8.9 and 10.2, respectively). In comparison, M. Pul1/ Post Central exhibits a lower degree of association with an enrichment factor of 7 and M. Pul2/ Middle Frontal Gyrus has the lowest spindle enrichment factor at 3.2. M. Pul2 and Middle Frontal Gyrus still appear to be highly related, but have a low enrichment factor, due to the skewing to the right of Middle Frontal Gyrus spindles. C. Downstate versus spindle. The M. Pul1/ Middle Frontal Gyrus pair shows that Middle Frontal Gyrus spindles occur during and just after the M. Pul1 downstate peak, with an enrichment factor of 5.3. Similarly, the Post Central spindles occur during the M. Pul2 downstate peak, with an enrichment factor of 4. Conversely, the opposite pairings show fairly flat histograms with low enrichment factors (2 for M. Pul2/ Middle Frontal Gyrus and 1.7 for M. Pul1/ Post Central). These plots demonstrate a double dissociation wherein one medial pulvinar contact pair is more closely related (in downstates, spindles, and their combination) to the middle frontal gyrus, and the other to the post central gyrus.

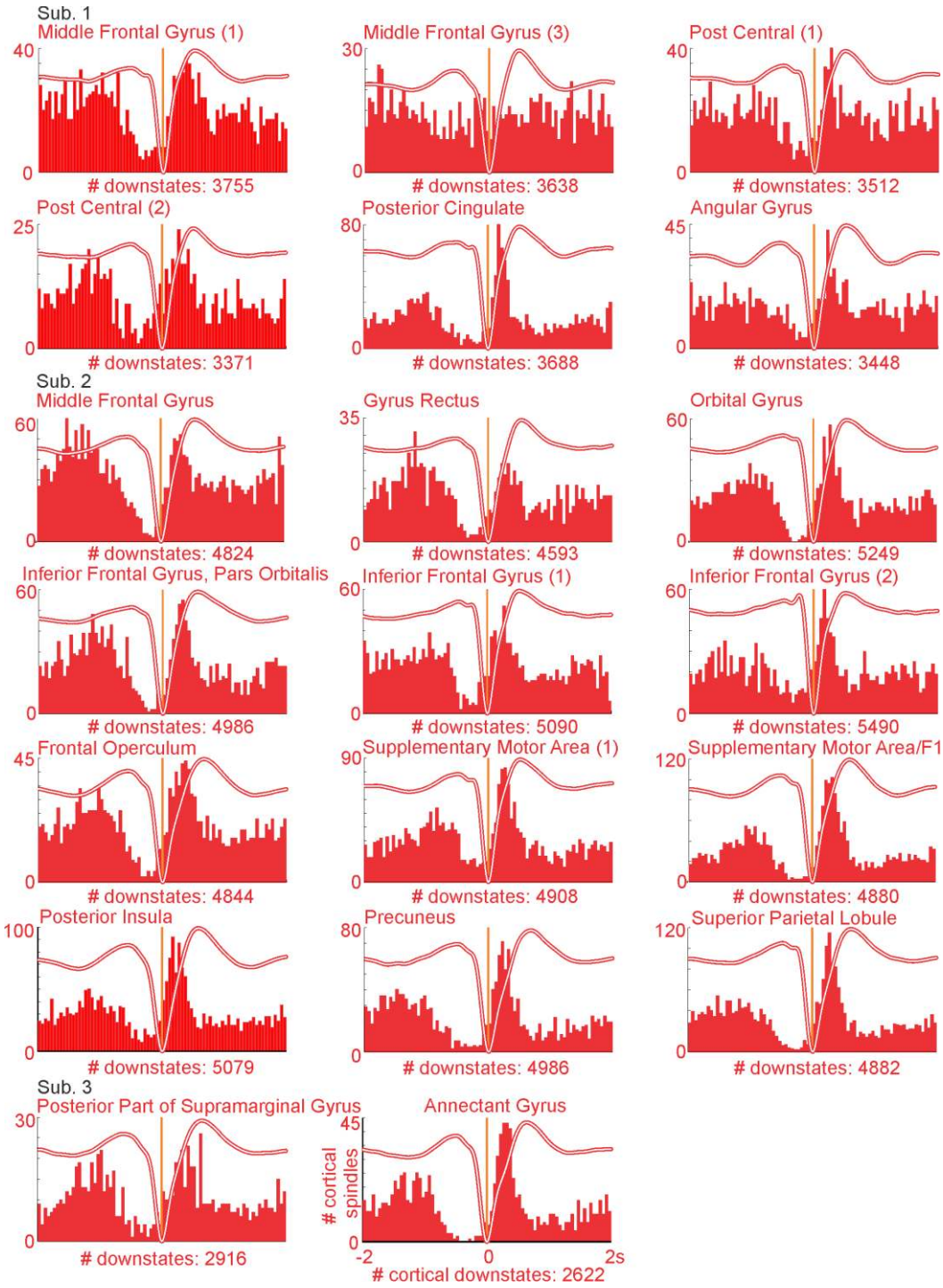

Supplementary Figure 9. Cortical spindles start during the cortical down-to-upstate transition. Cortical downstate peaks are locked at 0ms (vertical orange lines) and the corresponding cortical spindle onsets are plotted in red 50ms bins for each channel. Channels plotted here and in Fig. 4 comprise all cortical channels. Waveforms show the averaged local field potential in each channel.

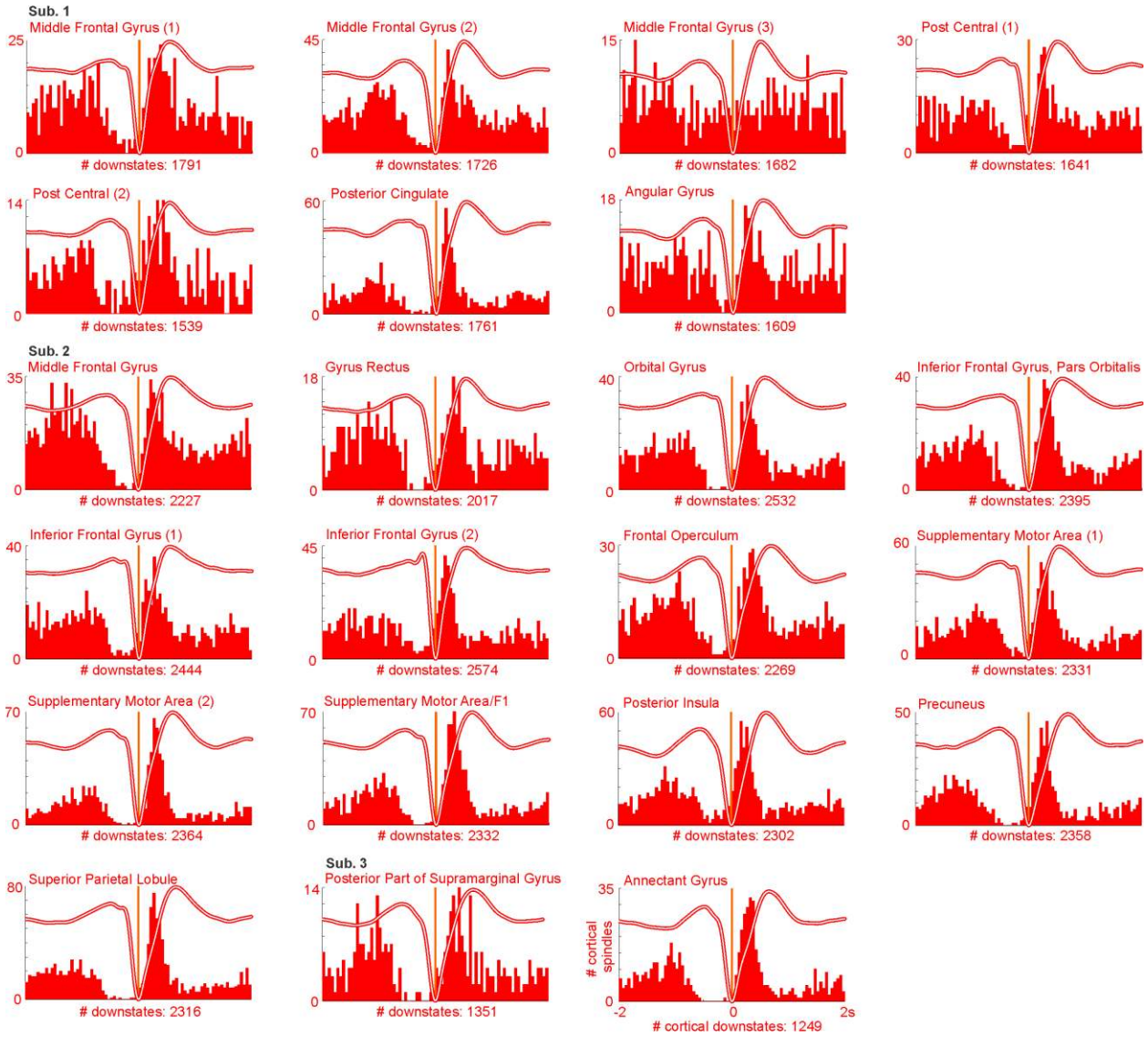

Supplementary Figure 10. Cortical spindles still start during the cortical down-to-upstate transition when stricter cortical downstate detection parameters are applied. When downstate detection parameters are changed to only select the bottom 20% of downstate peaks whose zero crossings occur between 0.25 to 1secs, the cortical spindles still start during the cortical down-to-upstate transition. Cortical downstate peaks are locked at 0ms (vertical orange lines) and the corresponding cortical spindle onsets are plotted in red 50ms bins for each channel. Waveforms show the averaged local field potential in each channel. All 22 cortical channels are plotted.

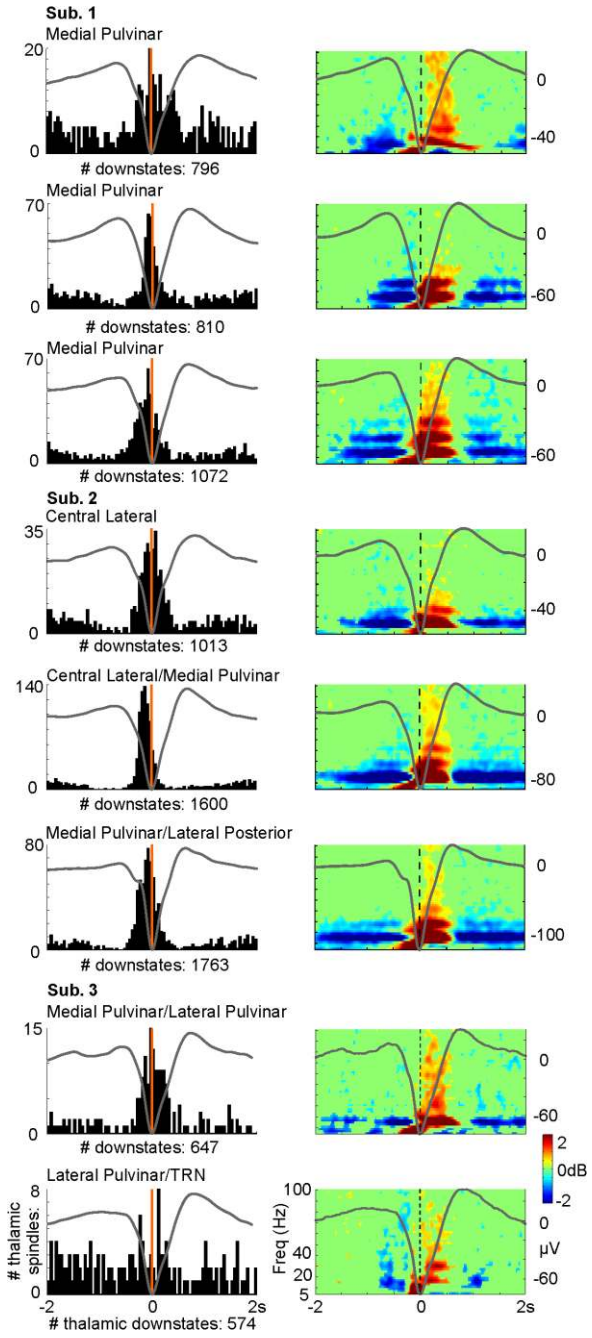

Supplementary Figure 11. Thalamic spindles still start at the thalamic downstate peak when stricter thalamic downstate detection parameters are applied. When downstate detection parameters are changed to only select the bottom 20% of downstate peaks whose zero crossings occur between 0.25 to 1secs, the thalamic spindles still start during the thalamic downstate. Histograms of thalamic spindle onsets (left column) in relation to the thalamic downstate peak at 0ms (vertical orange lines) for each thalamic channel in 50ms bins. Spectral power from 5-100Hz (right column), averaged on the downstate peaks at 0ms, baseline corrected over entire epoch, thresholded at $p<0.01$, uncorrected. All 8 thalamic channels are plotted. Waveforms show the averaged local field potential in each channel.

Subject 1	True Negative	False Negative	False Positive	True Positive	Hit Rate	False Alarm Rate	d'	C
Cortex								
Previous	1673	391	357	283	0.419881	0.175862	0.729	0.567
Current	1718	112	375	499	0.816694	0.179169	1.821	0.008
Thalamus								
Previous	303	166	151	451	0.730956	0.332599	1.048	-0.091
Current	398	94	89	490	0.839041	0.182752	1.895	-0.043
Subject 2	True Negative	False Negative	False Positive	True Positive	Hit Rate	False Alarm Rate	d'	C
Cortex								
Previous	3747	534	653	634	0.542808	0.148409	1.151	0.468
Current	3803	198	739	828	0.807018	0.162704	1.85	0.058
Thalamus								
Previous	454	100	176	468	0.823944	0.279365	1.515	-0.173
Current	561	75	90	472	0.862888	0.138249	2.182	-0.003
Subject 3	True Negative	False Negative	False Positive	True Positive	Hit Rate	False Alarm Rate	d'	C
Cortex								
Previous	213	182	21	156	0.461538	0.089744	1.246	0.72
Current	215	58	77	222	0.792857	0.263699	1.448	-0.092
Thalamus								
Previous	633	65	172	123	0.654255	0.213665	1.191	0.198
Current	705	27	137	124	0.821192	0.162708	1.903	0.032

Supplementary Table 1.

Discrimination table of the two spindle detection methods. For each subject, the calculations were performed over 10 minutes of N2 and 10 minutes of N3 that had been manually marked for spindles. Cortical and thalamic channels are considered separately for each subject. "Previous" refers to the method adapted from (*31*), which is described in the Methods. "Current" refers to our current spindle detection method. The Hit Rate was calculated by dividing the number of True Positives by the sum of the True Positives and False Negatives. The False Alarm Rate was calculated by dividing the number of False Positives by the sum of False Positives and True Negatives. True negatives in the current method were candidate epochs that were not automatically selected as spindles and were not manually marked as spindles. In order to approximate the number of true negatives in the previous method, the sum of the False Negatives, False Positives, and True Positives for the previous method was subtracted from the sum of the True Negatives, False Negatives, False Positives, and True Positives separately for the cortex and thalamus for each subject. The d', which measures discriminability, and C, which measures bias, were calculated using a d' calculator (http://memory.psych.mun.ca/models/dprime/).

A. Cortical channels							
Subject	**Channel Location**	**Downstate Density (/min) Overall**	**Spindle Density (/min) Overall**	**Downstate Density (/min) N2**	**Spindle Density (/min) N2**	**Downstate Density (/min) N3**	**Spindle Density (/min) N3**
Subject 1	Middle Frontal Gyrus (1)	17.63	4.80	11.10	3.09	29.39	7.87
	Middle Frontal Gyrus (2)	17.11	6.89	9.52	4.29	30.79	11.58
	Middle Frontal Gyrus (3)	17.08	4.65	9.82	4.66	30.17	4.63
	Post Central (1)	16.49	4.17	9.15	1.15	29.72	9.62
	Post Central (2)	15.83	3.03	10.86	2.93	24.78	3.21
	Posterior Cingulate	17.31	4.92	10.64	2.39	29.34	9.49
	Angular Gyrus	16.19	4.41	8.53	2.89	29.99	7.16
Subject 2	Middle Frontal Gyrus	15.87	6.13	8.36	4.58	25.65	8.14
	Gyrus Rectus	15.11	2.68	8.56	1.81	23.64	3.80
	Orbital Gyrus	17.27	4.28	11.08	2.69	25.33	6.36
	Inferior Frontal Gyrus, Pars Orbitalis	16.40	4.98	10.59	3.61	23.97	6.77
	Inferior Frontal Gyrus (1)	16.74	3.85	9.34	1.75	26.39	6.58
	Inferior Frontal Gyrus (2)	18.06	2.96	10.67	1.19	27.68	5.27
	Frontal Operculum	15.93	3.62	9.09	0.91	24.85	7.14
	Supplementary Motor Area (1)	16.14	6.19	9.10	3.97	25.33	9.08
	Supplementary Motor Area (2)	16.29	4.88	9.59	3.30	25.03	6.94
	Supplementary Motor Area/F1	16.05	6.62	9.67	4.05	24.37	9.97
	Posterior Insula	16.71	6.19	9.84	5.28	25.66	7.37
	Precuneus	16.40	4.70	10.31	2.91	24.33	7.05
	Superior Parietal Lobule	16.06	7.24	9.28	5.50	24.89	9.51
Subject 3	Posterior Part of Supramarginal Gyrus	14.58	4.89	11.26	3.69	20.36	6.96
	Annectant Gyrus	13.11	6.77	12.27	3.50	14.58	12.44
	Averages ± SD	16.29 ± 1.06	4.95 ± 1.33	9.94 ± 1.02	3.19 ± 1.30	25.74 ± 3.64	7.59 ± 2.30
B. Thalamic Channels							
Subject	**Channel Location**	**Downstate Density (/min)**	**Spindle Density (/min)**	**Downstate Density (/min) N2**	**Spindle Density (/min) N2**	**Downstate Density (/min) N3**	**Spindle Density (/min) N3**
Subject 1	Medial Pulvinar (1)	12.22	5.88	9.39	3.90	17.30	9.46
	Medial Pulvinar (2)	11.93	10.40	9.66	7.68	16.03	15.30
	Medial Pulvinar (3)	13.22	8.45	11.80	6.38	15.79	12.18
Subject 2	Central Lateral	10.75	6.29	9.78	3.52	12.02	9.89
	Central Lateral/ Medial Pulvinar	13.34	8.40	13.08	4.97	13.68	12.88
	Medial Pulvinar/ Lateral Posterior	13.49	6.73	14.09	4.59	12.72	9.52
Subject 3	Medial Pulvinar/ Lateral Pulvinar	8.98	5.41	10.65	4.09	6.07	7.71
	Lateral Pulvinar/ Nucleus Reticularis	7.64	5.24	9.13	4.59	5.04	6.37
	Averages ± SD	11.45 ± 2.17	7.10 ± 1.81	10.95 ± 1.85	4.96 ± 1.40	12.33 ± 4.55	10.41 ± 2.90

Supplementary Table 2.

Downstate and spindle densities (rate of occurrence) overall (N2 and N3 combined), and separately for N2 and N3. A. Downstate and spindle densities for individual cortical channels. B. Downstate and spindle densities for individual thalamic channels. When N2 and N3 are combined, all but one of the cortical channels exhibit overall downstates at a higher density than all of the thalamic channels. Conversely, thalamic channels tend to exhibit a higher overall spindle density than cortical channels. A two-way ANOVA comparing the downstate densities and spindle densities of the 22 cortical channels and 8 thalamic channels found a significant

main effect of the sleep event type (downstate or spindle, $p<0.0001$), a significant main effect of location (cortical or thalamic, $p<0.0023$), and a significant interaction effect ($p<0.0001$) on the frequency of these sleep events. The rare cortical channels that spindle more often than some individual thalamic channels were largely located in posterior areas, with two located in the middle frontal gyrus. Downstate and spindle densities overlapped more between cortical and thalamic channels during N2. Overall, however, in N3, downstate density was 2.1 times greater in cortical channels (25.74) than thalamic channels (12.33), while spindle density was about 1.4 times greater in thalamic channels (10.41) than cortical channels (7.59). In the cortical channels, both downstate (9.94 to 25.74) and spindle (3.19 to 7.59) densities increase between N2 and N3. In the thalamic channels, downstate density only slightly increases between N2 and N3 (10.95 to 12.33), while the spindle density more than doubles (4.96 to 10.41). Transitioning from N2 to N3, therefore, does not have much effect on downstate density in the thalamus, while it more than doubles the cortical downstate density. Conversely, transitioning from N2 to N3 increases spindle density in both the thalamus and the cortex, but spindling still occurs more often in the thalamus.

A. Downstates				B. Spindles			
A1. Cortex Leads Thalamus				**B1. Thalamus Leads Cortex**			
Subject	Leading channel location	Following channel location	p-value	Subject	Leading channel location	Following channel location	p-value
Subject 1	Middle Frontal Gyrus (1)	Medial Pulvinar (1)	p<0.000001	Subject 1	Medial Pulvinar (1)	Middle Frontal Gyrus (1)	p<0.000001
	Middle Frontal Gyrus (2)	Medial Pulvinar (1)	p<0.000001		Medial Pulvinar (1)	Middle Frontal Gyrus (2)	p<0.000001
	Middle Frontal Gyrus (3)	Medial Pulvinar (1)	p<0.000001		Medial Pulvinar (2)	Middle Frontal Gyrus (1)	p<0.000001
	Post Central (1)	Medial Pulvinar (1)	p<0.000001		Medial Pulvinar (2)	Middle Frontal Gyrus (2)	p<0.000001
	Posterior Cingulate	Medial Pulvinar (1)	p<0.000001		Medial Pulvinar (2)	Post Central (1)	p<0.000001
	Angular Gyrus	Medial Pulvinar (1)	p<0.000001		Medial Pulvinar (2)	Angular Gyrus	p<0.000001
	Middle Frontal Gyrus (1)	Medial Pulvinar (2)	p<0.000001		Medial Pulvinar (3)	Middle Frontal Gyrus (1)	p<0.000001
	Post Central (2)	Medial Pulvinar (2)	p<0.000001		Medial Pulvinar (3)	Middle Frontal Gyrus (2)	p<0.000001
	Middle Frontal Gyrus (1)	Medial Pulvinar (3)	p<0.000001		Medial Pulvinar (3)	Post Central (1)	p<0.000001
	Middle Frontal Gyrus (2)	Medial Pulvinar (3)	p<0.000001		Medial Pulvinar (3)	Angular Gyrus	0.00002
	Middle Frontal Gyrus (3)	Medial Pulvinar (3)	p<0.000001				
	Post Central (1)	Medial Pulvinar (3)	p<0.000001				
	Posterior Cingulate	Medial Pulvinar (3)	0.000008				
	Angular Gyrus	Medial Pulvinar (3)	p<0.000001				
Subject 2	Middle Frontal Gyrus	Central Lateral	p<0.000001	Subject 2	Central Lateral	Middle Frontal Gyrus	p<0.000001
	Gyrus Rectus	Central Lateral	0.00001		Central Lateral	Orbital Gyrus	p<0.000001
	Orbital Gyrus	Central Lateral	0.000182		Central Lateral	Pars Orbitalis	p<0.000001
	Pars Orbitalis	Central Lateral	0.000028		Central Lateral	Area (1)	0.000066
	Middle Frontal Gyrus	Central Lateral/ Medial Pulvinar	p<0.000001		Central Lateral	Supplementary Motor Area (2)	0.000083
	Supplementary Motor Area (1)	Central Lateral/ Medial Pulvinar	p<0.000001		Central Lateral/ Medial Pulvinar	Middle Frontal Gyrus	p<0.000001
	Posterior Insula	Central Lateral/ Medial Pulvinar	p<0.000001		Central Lateral/ Medial Pulvinar	Inferior Frontal Gyrus, Pars Orbitalis	0.000057
	Precuneus	Central Lateral/ Medial Pulvinar	0.000048		Central Lateral/ Medial Pulvinar	Supplementary Motor Area (1)	p<0.000001
	Middle Frontal Gyrus	Medial Pulvinar/ Lateral Posterior	0.000003		Central Lateral/ Medial Pulvinar	Supplementary Motor Area (2)	p<0.000001
	Supplementary Motor Area (1)	Medial Pulvinar/ Lateral Posterior	0.000001		Central Lateral/ Medial Pulvinar	Supplementary Motor Area/F1	p<0.000001
	Posterior Insula	Medial Pulvinar/ Lateral Posterior	0.000044		Central Lateral/ Medial Pulvinar	Superior Parietal Lobule	0.000242
Subject 3	Posterior Part of Supramar	Medial Pulvinar/ Lateral Pulvinar	p<0.000001		Medial Pulvinar/ Lateral Posterior	Middle Frontal Gyrus	p<0.000001
	Annectant Gyrus	Medial Pulvinar/ Lateral Pulvinar	p<0.000001		Medial Pulvinar/ Lateral Posterior	Orbital Gyrus	0.000117
	Annectant Gyrus	Lateral Pulvinar/ Nucleus Reticularis	p<0.000001		Medial Pulvinar/ Lateral Posterior	Inferior Frontal Gyrus, Pars Orbitalis	0.000002
				Subject 3	Medial Pulvinar/ Lateral Pulvinar	Posterior Part of Supramar	p<0.000001
					Medial Pulvinar/ Lateral Pulvinar	Annectant Gyrus	p<0.000001
					Lateral Pulvinar/ Nucleus Reticularis	Annectant Gyrus	p<0.000001
A2. Thalamus Leads Cortex				**B2. Cortex Leads Thalamus**			
Subject	Leading channel location	Following channel location	p-value	Subject	Leading channel location	Following channel location	p-value
Subject 1	Medial Pulvinar (2)	Middle Frontal Gyrus (3)	0.00001	None			
Subject 2	Central Lateral	Frontal Operculum	p<0.000001				
	Central Lateral	Supplementary Motor Area/F1	p<0.000001				
	Central Lateral	Posterior Insula	0.0005				

Supplementary Table 3.

Significant binomial tests over all subjects for downstate peaks and spindle starts between all thalamocortical pairs. Bonferroni correction at $p<0.05$ was applied over all thalamocortical pairs over all subjects, separately for downstates and spindles.

A. N2 Downstates				B. N2 Spindles			
A1. Cortex Leads Thalamus				**B1. Thalamus Leads Cortex**			
Subject	Leading channel	Following channel	p-value	Subject	Leading channel	Following channel	p-value
Subject 1	Middle Frontal Gyrus (1)	Medial Pulvinar (1)	p<0.000001	Subject 1	Medial Pulvinar (1)	Middle Frontal Gyrus (1)	0.000534
	Middle Frontal Gyrus (2)	Medial Pulvinar (1)	p<0.000001		Medial Pulvinar (2)	Middle Frontal Gyrus (1)	p<0.000001
	Middle Frontal Gyrus (3)	Medial Pulvinar (1)	p<0.000001		Medial Pulvinar (2)	Middle Frontal Gyrus (2)	p<0.000001
	Post Central (1)	Medial Pulvinar (1)	3.50E-05		Medial Pulvinar (2)	Post Central (1)	1.00E-04
	Posterior Cingulate	Medial Pulvinar (1)	1.20E-05		Medial Pulvinar (2)	Angular Gyrus	p<0.000001
	Angular Gyrus	Medial Pulvinar (1)	p<0.000001		Medial Pulvinar (3)	Middle Frontal Gyrus (1)	p<0.000001
	Middle Frontal Gyrus (1)	Medial Pulvinar (2)	p<0.000001		Medial Pulvinar (3)	Middle Frontal Gyrus (2)	p<0.000001
	Post Central (2)	Medial Pulvinar (2)	p<0.000001		Medial Pulvinar (3)	Middle Frontal Gyrus (3)	0.000257
	Middle Frontal Gyrus (1)	Medial Pulvinar (3)	p<0.000001		Medial Pulvinar (3)	Post Central (1)	1.00E-04
	Middle Frontal Gyrus (2)	Medial Pulvinar (3)	p<0.000001	Subject 2	Central Lateral	Middle Frontal Gyrus	p<0.000001
	Middle Frontal Gyrus (3)	Medial Pulvinar (3)	3.00E-06		Central Lateral	Orbital Gyrus	p<0.000001
	Post Central (1)	Medial Pulvinar (3)	p<0.000001		Central Lateral	Inferior Frontal Gyrus, Pars Orbitalis	p<0.000001
	Angular Gyrus	Medial Pulvinar (3)	0.000219		Central Lateral/ Medial Pulvinar	Middle Frontal Gyrus	p<0.000001
Subject 2	Middle Frontal Gyrus	Central Lateral	1.50E-05		Central Lateral/ Medial Pulvinar	Supplementary Motor Area (1)	p<0.000001
	Middle Frontal Gyrus	Central Lateral/ Medial Pulvinar	2.00E-06		Central Lateral/ Medial Pulvinar	Supplementary Motor Area (2)	p<0.000001
	Supplementary Motor Area (1)	Central Lateral/ Medial Pulvinar	p<0.000001		Central Lateral/ Medial Pulvinar	Supplementary Motor Area/F1	0.000257
	Posterior Insula	Central Lateral/ Medial Pulvinar	p<0.000001		Medial Pulvinar/ Lateral Posterior	Middle Frontal Gyrus	p<0.000001
	Posterior Insula	Medial Pulvinar/ Lateral Posterior	3.00E-06		Medial Pulvinar/ Lateral Posterior	Orbital Gyrus	0.000337
Subject 3	Posterior Part of Supramar	Medial Pulvinar/ Lateral Pulvinar	p<0.000001		Medial Pulvinar/ Lateral Posterior	Inferior Frontal Gyrus, Pars Orbitalis	1.30E-05
	Annectant Gyrus	Medial Pulvinar/ Lateral Pulvinar	p<0.000001		Medial Pulvinar/ Lateral Posterior	Supplementary Motor Area (1)	p<0.000001
	Annectant Gyrus	Lateral Pulvinar/ Nucleus Reticularis	p<0.000001	Subject 3	Medial Pulvinar/ Lateral Pulvinar	Posterior Part of Supramarginal Gyrus	p<0.000001
					Medial Pulvinar/ Lateral Pulvinar	Annectant Gyrus	2.00E-06
A2. Thalamus Leads Cortex				**B2. Cortex Leads Thalamus**			
Subject	Leading channel	Following channel	p-value	Subject	Leading channel	Following channel	p-value
Subject 2	Central Lateral	Frontal Operculum	5.00E-06	Subject 1	Post Central (2)	Medial Pulvinar (1)	0.000306
	Central Lateral	Supplementary Motor Area (1)	p<0.000001				
	Central Lateral	Supplementary Motor Area (2)	p<0.000001				
	Central Lateral	Supplementary Motor Area/F1	1.00E-06				

Supplementary Table 4.

Binomial tests for downstates and spindles for N2 only. The results are similar to N3 in Supplementary Table 5, and to the combined N2 and N3 results in Supplementary Table 3. The lone exception is the significant spindle binomial pair in Subject 1, where the post central channel leads the medial pulvinar channel in N2 (highlighted in yellow), but not in N3, or N2 and N3 combined.

A. N3 Downstates				B. N3 Spindles			
A1. Cortex Leads Thalamus				**B1. Thalamus Leads Cortex**			
Subject	Leading channel	Following channel	p-value	Subject	Leading channel	Following channel	p-value
Subject 1	Middle Frontal Gyrus (1)	Medial Pulvinar (1)	2.00E-06	Subject 1	Medial Pulvinar (1)	Middle Frontal Gyrus (1)	p<0.000001
	Middle Frontal Gyrus (2)	Medial Pulvinar (1)	p<0.000001		Medial Pulvinar (1)	Middle Frontal Gyrus (2)	p<0.000001
	Middle Frontal Gyrus (3)	Medial Pulvinar (1)	p<0.000001		Medial Pulvinar (2)	Middle Frontal Gyrus (1)	p<0.000001
	Post Central (1)	Medial Pulvinar (1)	p<0.000001		Medial Pulvinar (2)	Middle Frontal Gyrus (2)	p<0.000001
	Posterior Cingulate	Medial Pulvinar (1)	p<0.000001		Medial Pulvinar (2)	Post Central (1)	5.00E-06
	Angular Gyrus	Medial Pulvinar (1)	p<0.000001		Medial Pulvinar (3)	Middle Frontal Gyrus (1)	p<0.000001
	Middle Frontal Gyrus (1)	Medial Pulvinar (2)	p<0.000001		Medial Pulvinar (3)	Middle Frontal Gyrus (2)	p<0.000001
	Post Central (2)	Medial Pulvinar (2)	p<0.000001		Medial Pulvinar (3)	Post Central (1)	0.000152
	Middle Frontal Gyrus (1)	Medial Pulvinar (3)	p<0.000001	Subject 2	Central Lateral	Middle Frontal Gyrus	p<0.000001
	Middle Frontal Gyrus (2)	Medial Pulvinar (3)	p<0.000001		Central Lateral	Orbital Gyrus	5.90E-05
	Middle Frontal Gyrus (3)	Medial Pulvinar (3)	p<0.000001		Central Lateral	Inferior Frontal Gyrus, Pars Orbitalis	p<0.000001
	Post Central (1)	Medial Pulvinar (3)	p<0.000001		Central Lateral	Supplementary Motor Area (1)	0.000695
	Angular Gyrus	Medial Pulvinar (3)	2.30E-05		Central Lateral	Supplementary Motor Area (2)	0.000503
Subject 2	Middle Frontal Gyrus	Central Lateral	p<0.000001		Central Lateral/ Medial Pulvinar	Middle Frontal Gyrus	p<0.000001
	Gyrus Rectus	Central Lateral	p<0.000001		Central Lateral/ Medial Pulvinar	O'10-11	0.000673
	Orbital Gyrus	Central Lateral	0.000253		Central Lateral/ Medial Pulvinar	Supplementary Motor Area (1)	p<0.000001
	Inferior Frontal Gyrus, Pars Orbitalis	Central Lateral	5.00E-06		Central Lateral/ Medial Pulvinar	Supplementary Motor Area (2)	p<0.000001
	Middle Frontal Gyrus	Central Lateral/ Medial Pulvinar	p<0.000001		Central Lateral/ Medial Pulvinar	Supplementary Motor Area/F1	2.00E-06
	Supplementary Motor Area (1)	Central Lateral/ Medial Pulvinar	p<0.000001		Medial Pulvinar/ Lateral Posterior	Middle Frontal Gyrus	p<0.000001
	Posterior Insula	Central Lateral/ Medial Pulvinar	p<0.000001	Subject 3	Medial Pulvinar/ Lateral Pulvinar	Posterior Part of Supramarginal Gyrus	p<0.000001
	Precuneus	Central Lateral/ Medial Pulvinar	3.00E-06		Medial Pulvinar/ Lateral Pulvinar	Annectant Gyrus	p<0.000001
	Superior Parietal Lobule	Central Lateral/ Medial Pulvinar	2.10E-05		Lateral Pulvinar/ Nucleus Reticularis	Annectant Gyrus	p<0.000001
	Middle Frontal Gyrus	Medial Pulvinar/ Lateral Posterior	0.000227				
	Supplementary Motor Area (1)	Medial Pulvinar/ Lateral Posterior	1.90E-05				
Subject 3	Annectant Gyrus	Lateral Pulvinar/ Nucleus Reticularis	7.50E-05				
A2. Thalamus Leads Cortex				**B2. Cortex Leads Thalamus**			
Subject	Leading channel	Following channel	p-value	Subject	Leading channel	Following channel	p-value
Subject 1	Medial Pulvinar (2)	Inferior Frontal Gyrus (2)	0.000561	None			
Subject 2	Central Lateral	Frontal Operculum	9.50E-05				
	Central Lateral	Supplementary Motor Area/F1	0.000155				

Supplementary Table 5.

Binomial tests for downstates and spindles for N3 only. The results are similar to N2 in Supplementary Table 4, and to the combined N2 and N3 results in Supplementary Table 3.

A. Cortical channels				
Subject	**Channel Location**	**Proportion of Spindles with Downstates**	**Normalized Proportion of Spindles with Downstates**	**Enrichment Factor**
Subject 1	Middle Frontal Gyrus	0.38	0.38	2.46
	Middle Frontal Gyrus	0.40	0.42	2.87
	Middle Frontal Gyrus	0.21	0.21	1.35
	Post Central	0.38	0.41	3.28
	Post Central	0.32	0.36	2.82
	Posterior Cingulate	0.45	0.46	5.29
	Angular Gyrus	0.32	0.35	3.39
Subject 2	Middle Frontal Gyrus	0.28	0.32	2.11
	Gyrus Rectus	0.26	0.31	2.15
	Orbital Gyrus	0.33	0.35	3.04
	Inferior Frontal Gyrus, Pars Orbitalis	0.29	0.32	2.66
	Inferior Frontal Gyrus	0.37	0.4	3.19
	Inferior Frontal Gyrus	0.46	0.46	4.43
	Frontal Operculum	0.41	0.46	3.01
	Supplementary Motor Area	0.37	0.41	3.28
	Supplementary Motor Area	0.43	0.47	4.37
	Supplementary Motor Area/F1	0.41	0.46	3.79
	Posterior Insula	0.39	0.42	3.51
	Precuneus	0.36	0.4	3.63
	Superior Parietal Lobule	0.37	0.42	3.90
Subject 3	Posterior Part of Supramarginal Gyrus	0.23	0.23	1.94
	Annectant Gyrus	0.24	0.27	2.91
	Averages ± SD	0.35 ± 0.07	0.38 ± 0.07	3.15 ± 0.9
B. Thalamic channels				
Subject	**Channel Location**	**Proportion of Spindles with Downstates**	**Normalized Proportion of Spindles with Downstates**	**Enrichment Factor**
Subject 1	Medial Pulvinar	0.39	0.56	4.63
	Medial Pulvinar	0.39	0.57	5.90
	Medial Pulvinar	0.56	0.74	5.80
Subject 2	Central Lateral	0.42	0.70	5.26
	Central Lateral/ Medial Pulvinar	0.69	0.94	9.86
	Medial Pulvinar/ Lateral Posterior	0.60	0.80	6.43
Sbuject 3	Medial Pulvinar/ Lateral Pulvinar	0.30	0.49	4.82
	Lateral Pulvinar/ Nucleus Reticularis	0.14	0.26	2.25
	Averages ± SD	0.43 ± 0.18	0.63 ± 0.21	5.62 ± 2.13

Supplementary Table 6.

Downstates strongly modulate spindles in the thalamus compared to the cortex. The number of spindles occurring with downstates was calculated for each channel. Due to their different relationship to downstate peaks, slightly different timing criteria were used for cortical

(A) and thalamic (B) channels: 0-750ms around the downstate peak for cortical channels and -500ms to + 250ms around the downstate peak for thalamic channels. The proportion of spindles occurring with downstates was then calculated by dividing the number of spindles that occurred within these specified time windows divided by the total number of spindles. The thalamic channels exhibited a higher proportion of downstate-related spindles (0.43 ± 0.18) compared to cortical channels (0.35 ± 0.07). When these proportions were normalized to account for the larger number of downstates occurring in the cortex (see Methods), the normalized proportion of spindles occurring with downstates is even larger between thalamic channels (0.63 ± 0.21) and cortical channels (0.38 ± 0.07). The enrichment factor measures how spindle density increases in a channel when spindles occur in relation to downstates compared to the channel's overall spindle density (see Methods). The thalamic channels show greater enrichment factors (5.62 ± 2.13) compared to the cortical channels (3.15 ± 0.9), further indicating that spindles in the thalamus are more highly modulated by the downstate than in the cortex.

Supplementary Note 1. Convergence of cortical downstates leads to a thalamic downstate

The binomial results indicate a statistically significant tendency for cortical downstates to lead thalamic downstates; however, examination of connected thalamocortical pairs still finds that the number of cortical downstates leading to thalamic downstates remains low (Supplementary Figure 2A, boxed histograms). For example, even though the posterior insula downstates strikingly cluster just prior to the central lateral/medial pulvinar downstates, only 1258 out of 5079 posterior insula downstates, or ~25%, are followed by central lateral/medial pulvinar downstates within 500ms. The annectant gyrus and medial/lateral pulvinar pair also exhibit downstates that are tightly coupled in time to one another; however, only 400, or ~15% of the 2622 downstates in the annectant gyrus are followed by downstates in the medial/lateral pulvinar. We therefore hypothesized that a convergence of cortical downstates may be required for thalamic downstates to occur. Due to limited cortical sampling, however, a complete examination of this hypothesis is also limited. For the following analyses, only cortical bipolar pairs that were separated by at least two contacts were included.

The hypothesis that convergence from multiple cortical downstates induces thalamic downstates was tested in three ways. First, the percentage of thalamic downstates without a prior cortical downstate (in any cortical channel) within 500ms was examined for each thalamic channel. It was predicted that if a subject has more cortical channels, the percentage of isolated thalamic downstates would decrease. Subject 3 only had two cortical channels and consistent with this prediction, both thalamic channels showed a high percentage of downstates without a preceding downstate in at least one cortical channel: 67% for the Medial/Lateral Pulvinar channel and 89% for the Lateral Pulvinar/Nucleus Reticularis channel. Subject 1 included six cortical channels and Subject 2 included ten cortical channels. In both subjects, the percentage of isolated thalamic downstates decreased by ~50% compared with Subject 3: 37%, 39%, and 42% for each of the three Medial Pulvinar channels in Subject 1, with a continued drop to 35% for the Central Lateral, 30% for the Central Lateral/Medial Pulvinar, and 36% for the Medial Pulvinar/Lateral Posterior channels in Subject 2. We would predict that with robust cortical sampling, thalamic downstates would not occur without preceding cortical downstates.

Second, we examined whether cortical pairs that produce downstates together are more likely to lead to thalamic downstates, compared with cortical downstates produced in only one of

these cortical channels. For each pair of cortical channels, the number of downstates occurring within 500ms of the locked channel was calculated. The probability of thalamic downstates occurring within 500ms after these paired cortical downstates was calculated for each thalamic channel; the downstate peak of the locked cortical channel was used to search for thalamic downstates. The probability of thalamic downstates in each thalamic channel occurring within 500ms of isolated cortical downstates was also calculated for each cortical channel individually. Over all thalamic channels, the mean probability of thalamic downstates occurring with cortical pairs (0.14) was significantly greater than when thalamic downstates occur with a single cortical channel (0.10) (paired t-test, $p=0.011$, 8 thalamic channels). A Chi-squared test was performed between the proportion of thalamic downstates relative to isolated versus paired cortical downstates. Out of 364 unique cortical /thalamic channel combinations, 54 (~15%) were significant after Bonferroni correction at $p<0.05$. For an example, see Fig. 1G (in the main text). Of these, one showed a greater probability of a thalamic downstate when downstates occurred on the individual cortical channel, but the remaining 53 showed a greater probability of a thalamic downstate when the cortical downstate occurred in both cortical channels. Overall, these results indicate that thalamic downstates are more likely to occur when cortical downstates occur in two related cortical channels.

The third way we tested the convergence hypothesis was by examining the probability of a thalamic downstate as a function of the number of cortical channels showing a downstate. With small and occasional exceptions, the addition of multiple channels participating in a cortical downstate further increased the probability of a following thalamic downstate, as shown in Supplementary Figure 3. In summary, our results indicate that as a greater number of related cortical channels participate in a downstate, the more likely a downstate will follow in the thalamus. Overall, however, the percentages are relatively low. This may suggest that very widespread convergence is needed, which was not possible to observe given our limited cortical sampling. Alternatively, upstates or another ongoing process not measured here may also be contributing to the generation of thalamic downstates.

Supplementary Note 2. Corticothalamic pair connectivity

A total of 64 unique corticothalamic pairs were sampled over all three patients. Two of these pairs were located in areas previously shown to be anatomically and functionally connected (*52-54*): the medial pulvinar and the posterior insula, and the pulvinar and the annectant gyrus (intraparietal sulcus). Both of these pairs exhibited unique relationships during downstates and spindles, which are featured in Supplementary Figure 2 (boxed histograms) and Fig. 3C-E.

Additional pairs also demonstrated differing degrees of functional specificity, supporting growing evidence that cortico-pulvinar connections may be variable even within the medial pulvinar (*52, 55*). Within the medial pulvinar of Subject 1, we find a double dissociation where one medial pulvinar channel is highly associated with a middle frontal gyrus channel and a second medial pulvinar channel is highly associated with a post central channel. This relationship is detailed in Supplementary Figure 8.

1. M. Steriade, A. Nunez, F. Amzica, A novel slow (< 1 Hz) oscillation of neocortical neurons in vivo: depolarizing and hyperpolarizing components. *J. Neurosci.* **13**, 3252 (Aug, 1993).
2. J. Y. Chen, S. Chauvette, S. Skorheim, I. Timofeev, M. Bazhenov, Interneuron-mediated inhibition synchronizes neuronal activity during slow oscillation. *J Physiol* **590**, 3987 (Aug 15, 2012).
3. D. A. McCormick, T. Bal, Sleep and arousal: thalamocortical mechanisms. *Annu. Rev. Neurosci.* **20**, 185 (1997).
4. D. A. McCormick, M. J. McGinley, D. B. Salkoff, Brain state dependent activity in the cortex and thalamus. *Curr. Opin. Neurobiol.* **31**, 133 (Apr, 2015).
5. R. S. Morison, D. L. Bassett, *Electrical activity of the thalamus and basal ganglia in decorticate cats*. (1945), vol. 8, pp. 309-314.
6. M. Steriade, A. Nunez, F. Amzica, Intracellular analysis of relations between the slow (< 1 Hz) neocortical oscillation and other sleep rhythms of the electroencephalogram. *The Journal of neuroscience : the official journal of the Society for Neuroscience* **13**, 3266 (Aug, 1993).
7. F. David *et al.*, Essential thalamic contribution to slow waves of natural sleep. *J. Neurosci.* **33**, 19599 (Dec 11, 2013).
8. M. Lemieux, J. Y. Chen, P. Lonjers, M. Bazhenov, I. Timofeev, The impact of cortical deafferentation on the neocortical slow oscillation. *J. Neurosci.* **34**, 5689 (Apr 16, 2014).
9. M. Bonjean *et al.*, Corticothalamic feedback controls sleep spindle duration in vivo. *J. Neurosci.* **31**, 9124 (Jun 22, 2011).
10. D. Contreras, M. Steriade, Cellular basis of EEG slow rhythms: a study of dynamic corticothalamic relationships. *J. Neurosci.* **15**, 604 (Jan, 1995).
11. M. Molle, L. Marshall, S. Gais, J. Born, Grouping of spindle activity during slow oscillations in human non-rapid eye movement sleep. *J. Neurosci.* **22**, 10941 (Dec 15, 2002).
12. T. Andrillon *et al.*, Sleep spindles in humans: insights from intracranial EEG and unit recordings. *J. Neurosci.* **31**, 17821 (Dec 7, 2011).
13. F. P. Battaglia, G. R. Sutherland, B. L. McNaughton, Hippocampal sharp wave bursts coincide with neocortical "up-state" transitions. *Learn Mem* **11**, 697 (Nov-Dec, 2004).
14. A. G. Siapas, M. A. Wilson, Coordinated interactions between hippocampal ripples and cortical spindles during slow-wave sleep. *Neuron* **21**, 1123 (Nov, 1998).
15. L. A. Johnson, D. R. Euston, M. Tatsuno, B. L. McNaughton, Stored-trace reactivation in rat prefrontal cortex is correlated with down-to-up state fluctuation density. *The Journal of neuroscience : the official journal of the Society for Neuroscience* **30**, 2650 (Feb 17, 2010).
16. M. Molle, O. Yeshenko, L. Marshall, S. J. Sara, J. Born, Hippocampal sharp wave-ripples linked to slow oscillations in rat slow-wave sleep. *J. Neurophysiol.* **96**, 62 (Jul, 2006).
17. N. Maingret, G. Girardeau, R. Todorova, M. Goutierre, M. Zugaro, Hippocampo-cortical coupling mediates memory consolidation during sleep. *Nat. Neurosci.*, (May 16, 2016).
18. B. P. Staresina *et al.*, Hierarchical nesting of slow oscillations, spindles and ripples in the human hippocampus during sleep. *Nat Neurosci*, (Sep 21, 2015).
19. M. Niknazar, G. P. Krishnan, M. Bazhenov, S. C. Mednick, Coupling of Thalamocortical Sleep Oscillations Are Important for Memory Consolidation in Humans. *PloS one* **10**, e0144720 (2015).

20. R. A. Mak-McCully *et al.*, Distribution, Amplitude, Incidence, Co-Occurrence, and Propagation of Human K-Complexes in Focal Transcortical Recordings(1,2,3). *eNeuro* **2**, (Jul-Aug, 2015).
21. R. Csercsa *et al.*, Laminar analysis of slow wave activity in humans. *Brain* **133**, 2814 (Sep, 2010).
22. E. G. Jones, Synchrony in the interconnected circuitry of the thalamus and cerebral cortex. *Ann. N. Y. Acad. Sci.* **1157**, 10 (Mar, 2009).
23. R. A. Mak-McCully *et al.*, Synchronization of isolated downstates (K-complexes) may be caused by cortically-induced disruption of thalamic spindling. *PLoS Comput Biol* **10**, e1003855 (Sep, 2014).
24. P. Bartho *et al.*, Ongoing network state controls the length of sleep spindles via inhibitory activity. *Neuron* **82**, 1367 (Jun 18, 2014).
25. G. P. Krishnan *et al.*, Cellular and neurochemical basis of sleep stages in the thalamocortical network. *Elife* **5**, (Nov 16, 2016).
26. M. Biel, C. Wahl-Schott, S. Michalakis, X. Zong, Hyperpolarization-activated cation channels: from genes to function. *Physiol. Rev.* **89**, 847 (Jul, 2009).
27. S. Ray, N. E. Crone, E. Niebur, P. J. Franaszczuk, S. S. Hsiao, Neural correlates of high-gamma oscillations (60-200 Hz) in macaque local field potentials and their potential implications in electrocorticography. *J. Neurosci.* **28**, 11526 (Nov 05, 2008).
28. N. Kraus, T. Nicol, in *Encyclopedia of Neuroscience,* M. Binder, N. Hirokawa, U. Windhorst, Eds. (Springer Berlin Heidelberg, 2009), pp. 214-218.
29. I. Timofeev, M. Steriade, Low-frequency rhythms in the thalamus of intact-cortex and decorticated cats. *J. Neurophysiol.* **76**, 4152 (1996).
30. M. Steriade, Grouping of brain rhythms in corticothalamic systems. *Neuroscience* **137**, 1087 (2006).
31. Y. Nir *et al.*, Regional slow waves and spindles in human sleep. *Neuron* **70**, 153 (Apr 14, 2011).
32. A. Crespel, P. Coubes, M. Baldy-Moulinier, Sleep influence on seizures and epilepsy effects on sleep in partial frontal and temporal lobe epilepsies. *Clin Neurophysiol* **111 Suppl 2**, S54 (Sep, 2000).
33. L. Marshall, H. Helgadottir, M. Molle, J. Born, Boosting slow oscillations during sleep potentiates memory. *Nature* **444**, 610 (Nov 30, 2006).
34. S. C. Mednick *et al.*, The critical role of sleep spindles in hippocampal-dependent memory: a pharmacology study. *J. Neurosci.* **33**, 4494 (Mar 6, 2013).
35. R. Huber, M. F. Ghilardi, M. Massimini, G. Tononi, Local sleep and learning. *Nature* **430**, 78 (Jul 1, 2004).
36. B. Rasch, J. Born, About sleep's role in memory. *Physiol. Rev.* **93**, 681 (Apr, 2013).
37. D. Ji, M. A. Wilson, Coordinated memory replay in the visual cortex and hippocampus during sleep. *Nat. Neurosci.* **10**, 100 (Jan, 2007).
38. A. Sirota, J. Csicsvari, D. Buhl, G. Buzsaki, Communication between neocortex and hippocampus during sleep in rodents. *Proc Natl Acad Sci U S A* **100**, 2065 (Feb 18, 2003).
39. M. Steriade, I. Timofeev, F. Grenier, Natural waking and sleep states: a view from inside neocortical neurons. *J. Neurophysiol.* **85**, 1969 (May, 2001).

40. J. Talairach, P. Tournoux, *Co-planar stereotaxic atlas of the human brain: 3-dimensional proportional system: an approach to cerebral imaging*. (Thieme, Stuttgart, Germany, 1998).
41. H. Duvernoy, *The Human Brain: Surface, Blood Supply, and Three-Dimensional Sectional Anatomy*. (Springer, ed. 2nd, 1999).
42. A. Morel, M. Magnin, D. Jeanmonod, Multiarchitectonic and stereotactic atlas of the human thalamus. *J. Comp. Neurol.* **387**, 588 (Nov 3, 1997).
43. B. A. Riedner *et al.*, Sleep homeostasis and cortical synchronization: III. A high-density EEG study of sleep slow waves in humans. *Sleep* **30**, 1643 (Dec, 2007).
44. M. Ushimaru, Y. Ueta, Y. Kawaguchi, Differentiated participation of thalamocortical subnetworks in slow/spindle waves and desynchronization. *J. Neurosci.* **32**, 1730 (Feb 1, 2012).
45. V. Crunelli, M. L. Lorincz, A. C. Errington, S. W. Hughes, Activity of cortical and thalamic neurons during the slow (<1 Hz) rhythm in the mouse in vivo. *Pflugers Arch* **463**, 73 (Jan, 2012).
46. M. Kutner, C. Nachtsheim, J. Neter. (McGraw Hill Education, 2004).
47. R. R. Hocking, A Biometrics Invited Paper. The Analysis and Selection of Variables in Linear Regression. *Biometrics* **32**, 1 (1976).
48. P. C. Austin, J. V. Tu, Bootstrap Methods for Developing Predictive Models. *The American Statistician* **58**, 131 (2004).
49. R Development Core Team. (R Foundation for Statistical Computing, Vienne, Austria, 2004).
50. MATLAB, *version 8.3.0.532 (R2014a)*. (The MathWorks Inc., 2014).
51. A. Delorme, S. Makeig, EEGLAB: an open source toolbox for analysis of single-trial EEG dynamics including independent component analysis. *J. Neurosci. Methods* **134**, 9 (Mar 15, 2004).
52. M. J. Arcaro, M. A. Pinsk, S. Kastner, The Anatomical and Functional Organization of the Human Visual Pulvinar. *J. Neurosci.* **35**, 9848 (Jul 8, 2015).
53. E. J. Mufson, M. M. Mesulam, Thalamic connections of the insula in the rhesus monkey and comments on the paralimbic connectivity of the medial pulvinar nucleus. *J. Comp. Neurol.* **227**, 109 (Jul 20, 1984).
54. D. S. Rosenberg, F. Mauguiere, H. Catenoix, I. Faillenot, M. Magnin, Reciprocal thalamocortical connectivity of the medial pulvinar: a depth stimulation and evoked potential study in human brain. *Cereb. Cortex* **19**, 1462 (Jun, 2009).
55. M. Thieffry, Y. Burnod, Y. Poussart, J. Calvet, Synchronous modifications in the cortical and pulvinar unit activity during slow wave sleep. *Exp. Neurol.* **55**, 327 (May, 1977).